UHASSELT
KNOWLEDGE IN ACTION

Maastricht University

Faculty of Medicine and Life Sciences
School for Life Sciences
Master of Biomedical Sciences

Master's thesis

Exploring potential genes linked to dilated cardiomyopathy in zebrafish

Flore Hermans

Thesis presented in fulfillment of the requirements for the degree of Master of Biomedical Sciences, specialization Molecular Mechanisms in Health and Disease

SUPERVISOR :

Dr. Jo VANOEVELEN

2024
2025

Transnational University Limburg is a unique collaboration of two universities in two countries: the University of Hasselt and Maastricht University.

UHASSELT
KNOWLEDGE IN ACTION

www.uhasselt.be
Universiteit Hasselt
Campus Hasselt:
Martelarenlaan 42 | 3500 Hasselt
Campus Diepenbeek:
Agoralaan Gebouw D | 3590 Diepenbeek

UHASSELT
KNOWLEDGE IN ACTION

Maastricht University

Faculty of Medicine and Life Sciences
School for Life Sciences
Master of Biomedical Sciences

Master's thesis

Exploring potential genes linked to dilated cardiomyopathy in zebrafish

Flore Hermans

Thesis presented in fulfillment of the requirements for the degree of Master of Biomedical Sciences, specialization Molecular Mechanisms in Health and Disease

SUPERVISOR :

Dr. Jo VANOEVELEN

Exploring potential genes linked to dilated cardiomyopathy in zebrafish

F.J.H. Hermans[1], J. Grashorn[2], E. Lambrichs[2] and J. Vanoevelen[2]

[1]Universiteit Hasselt, Campus Diepenbeek, Agoralaan Gebouw C - B-3590 Diepenbeek
[2]Clinical Genetics, MUMC+, University of Maastricht, Campus Randwyck, UNS50 – 6202 AZ Maastricht

*Running title: *Exploring genes linked to DCM in zebrafish*

To whom correspondence should be addressed: Dr. J. Vanoevelen, Tel: +32 433 88 29 82 ; Email: j.vanoevelen@maastrichtuniversity.nl

Keywords: Dilated Cardiomyopathy, zebrafish, *LAPTM4B*, *PIGV*, *ANKHD1*, F0 screening, CRISPR/Cas9.

ABSTRACT

Dilated cardiomyopathy (DCM) is a leading cause of heart failure worldwide, and is characterized by a dysfunctional and dilated left ventricle. Approximately 1 in 250 individuals develop DCM in their lifetime. DCM is highly heritable, with around 50 associated genes. However, 60-75% of families that show a heritable DCM pattern have no genetic diagnosis. Thus, identifying novel DCM-associated genes is imperative to help diagnose patients earlier and provide personalized treatments based on genotype-phenotype associations. Previously, whole exome sequencing data from idiopathic DCM patients at Maastricht Hospital was analyzed, leading to the identification of three potentially DCM-causing genes, found in seven patients. In the current study, these genes were analyzed using the zebrafish model. It was hypothesized that the targeted knockout of *LAPTM4B*, *PIGV*, or *ANKHD1* in zebrafish embryos leads to functional and morphological changes resembling DCM. With F0 screening, a CRISPR/Cas9 based method, functional knockouts were created showing mild/moderate edema in approximately 40% of embryos in each genetic knockout. Heart videos were made to assess functional changes, with *laptm4b* showing a decrease in heart rate and an increase in ejection fraction, *pigv* showing a decrease in relaxation time and ventricle size, and *ankhd1* showing an increase in ventricle size. In conclusion, the F0 screening should be further optimized to fully assess the role of these genes in cardiomyopathy. This study gives a proof of concept, showing that *LAPTM4B*, *PIGV*, and *ANKHD1* play a role in the function and morphology of the heart and should be researched further.

1. INTRODUCTION

Dilated cardiomyopathy (DCM) is one of the leading causes of heart failure, affecting approximately 1 in 250 individuals during their lifetime (1, 2). It is a heart muscle disease, characterized by left ventricle (LV) dilation and contractile dysfunction, in absence of abnormal loading conditions or coronary artery disease sufficient to explain the dysfunction (3, 4). A DCM heart shows a patchwork of cardiomyocytes, fibrosis, necrosis and calcifications, which collectively contribute to elevated diastolic pressure. Initially, the heart compensates for this through neurohumoral activation, for example through the renin-angiotensin-aldosterone system (1). However, prolonged activation has adverse effects on cardiac function, and may exacerbate heart failure and edema (5). The full pathophysiology of DCM involves numerous pathways, many of which remain poorly understood (1).

DCM patients typically develop symptoms between 20 and 60 years of age, with symptoms including typical signs of heart failure like dyspnea, peripheral edema and reduced exercise capacity, and arrhythmias. Additionally, some types of DCM make patients more vulnerable to thromboembolic events and sudden cardiac death (SCD) (1). Patients are mostly diagnosed after the onset of symptoms. However, detection in the pre-symptomatic stage can delay adverse remodeling, prevent heart failure symptoms, and increase life expectancy for

patients, underscoring the importance of early detection (2). A DCM diagnosis is made based on exclusion of other diseases, environmental factors, family history and clinical examinations (2-4, 6). These clinical examinations typically include an echo or cardiac magnetic resonance imaging (CMR), which are necessary to asses LV volumes and LV ejection fraction (LVEF) (2, 4). A DCM diagnosis may be considered when LVEF <45%, end diastolic volume (EDV) index >117%, and fractional shortening is <25% (7). Additionally, CMR can detect adverse remodeling characteristics such as myocardial fibrosis, functional mitral regurgitation, and enlargement of other chambers, all of which aid in determining prognosis (2). Patients can manage DCM through pharmacologic therapy (e.g. ACE inhibitors, angiotensin receptor blockers, β-blockers), low-to-moderate exercise, and devices like the implantable cardioverter defibrillator (ICD) (3). Without treatment, the one-year survival rate is 70-75% and the five-year survival rate 50%, with most deaths attributed to pump failure and SCD (1).

DCM can be classified into several types. Secondary, or acquired, DCM is caused by environmental influences like alcohol abuse or pregnancy. Primary idiopathic DCM has no identifiable cause and primary familial DCM is attributed to genetic factors (1, 3). However, these categories of DCM are not mutually exclusive. There is growing evidence supporting an interactive model, in which environmental influences act as triggers for genetic variants, leading to DCM development (8). To adjust for these interactions the World Heart Federation has developed a new classification scheme for DCM, called MOGE(S), which takes different aspects of the disease into account (9).

DCM is highly heritable, with disease-causing genetic variants identified in 30-40% of patients. The majority of disease genes follow mostly monogenic, autosomal dominant inheritance pattern. However, in rare cases, X-linked, autosomal recessive, and mitochondrial inheritance are also observed. Monogenic DCM shows both locus and allelic heterogeneity and exhibits age-dependent penetrance (3). Mutations are predominantly identified in genes related to the cytoskeleton (e.g. *DES*), the cardiomyocyte sarcomeres (e.g. *TTN*tv, *FLNC*) and nuclear envelope proteins (e.g. *LMNA*) (1). Truncated titin variants (*TTN*tv) are the most common cause of both familial and sporadic DCM, accounting for approximately 25% of all autosomal dominant DCM cases (1, 10). Titin (*TTN*) encodes the largest protein expressed in mammals, generating stretch-resisting force, restoring the sarcomere to its resting length (10). *TTN* mutations have been shown to be more prevalent in patients with late onset (>40y) DCM (1). Another commonly affected gene is Lamin A/C (*LMNA*), which encodes type A and type C Lamins, which serve as a connective and mechanosensory network surrounding the nucleus, influences actin formation and plays a role in many well-known pathways like the Hippo pathway (11). *LMNA* mutations account for approximately 5% of autosomal dominant DCM cases and are associated with a higher incidence of conduction diseases, likely due to their impact on the interventricular septum, a critical structure for electrical conduction (1, 8, 12). As a result, patients are at higher risk for SCD, warranting a prophylactic ICD implantation. *LMNA* mutations have also been linked to arterial and venous thromboembolism, even in asymptomatic carriers (12). Additionally, *LMNA* related DCM has a poorer prognosis than other forms of DCM, leading to end-stage heart failure and requiring heart transplantation (7). Lastly, filamin C (*FLNC*) is another well-known DCM disease gene and encodes a structural, actin-crosslinking protein, which provides mechanical support for the sarcomere (13). *FLNC* mutations account for 1-5% of all autosomal dominant DCM cases. Patients with these mutations show a strong arrhythmogenic trait and a higher prevalence of SCD, making them also more likely to qualify for a prophylactic ICD implantation (1, 3, 13). In addition to the aforementioned genes, over 50 genes have been associated with DCM, with their own specific genotype-phenotype correlations (3).

The evolution of next generation sequencing (NGS) over recent years has enabled screening of these genetic variants in patients. In clinical diagnostics, gene panels targeting known DCM-associated genes are used for familial screenings of DCM patients, leading to earlier diagnosis and treatment. However, 60-75% of families exhibiting a clear autosomal dominant DCM inheritance

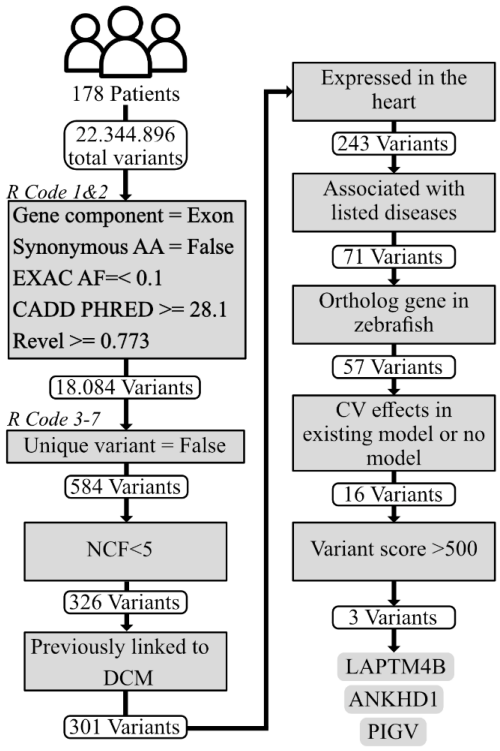

Figure 1 – Filtering process of genetic variants. *Whole exome sequencing data was collected from 178 patients, yielding 22 million variants. An initial automated filtering step, conducted with seven custom R scripts, resulted in 18.084 variants. Manual analysis further excluded variants until three genes were left, namely LAPTM4B, ANKHD1 and PIGV. Listed diseases included mitochondrial disease, muscular dystrophy, epilepsy, diseases with cardiac implications, or upregulation in cancer. AA, amino acid; EXAC AF, Exome Aggregation Consortium allele frequency; CADD PHRED, Combined Annotation Dependent Depletion PHRED-Like score; Revel, rare exome variant ensemble learner; NCF, non-causative frequency; DCM, dilated cardiomyopathy; CV, cardiovascular; LAPTM4B, lysosomal-associated transmembrane protein 4 beta; ANKHD1, ankyrin repeat and KH domain containing 1; PIGV, phosphatidylinositol glycan anchor biosynthesis class V.*

pattern are left without a genetic diagnosis. Thus, identifying novel disease-causing variants is crucial to expand these gene panels and diagnose patients earlier (3, 6). Whole exome sequencing (WES) allows the discovery of novel variants, since the entire exome is sequenced. Found variants can be labelled as pathogenic, likely-pathogenic, likely-benign, benign and unknown pathogenicity. Only variants classified as pathogenic or likely-pathogenic are considered clinically significant. The variants of unknown pathogenicity lack the evidence to be correctly classified and are also termed variants of unknown significance (VUS). These VUS are a good entry point to novel genes and gene variants for further research (6).

At Maastricht University Hospital, a cohort of 178 idiopathic DCM patients was selected from a cardiac patient database, based on the absence of an identifiable cause for their DCM. Between 2018 and 2022, these patients underwent WES, yielding approximately 22 million variants, which were subsequently filtered to uncover potential novel causative genes. First, the raw WES data underwent processing steps including quality control, post alignment processing, variant calling and annotation. The resulting 22 million variants were filtered through seven R scripts, which were based on allele frequency, CADD PHRED score, Revel score (14-17), and all unique variants were removed. This resulted in 584 variants, which were then subjected to a manual filtering step. This step included variants with a NCF>5, a variant score >500, no previous association with DCM, expression in the heart, association with diseases that have been linked to syndromic DCM and if they had an orthologue in zebrafish. Additionally, existing genetic models in mice and zebrafish were checked for cardiovascular defects, genes without such phenotypes were excluded (Fig. 1). This filtering process resulted in the three genes of interest for this study, namely lysosomal-associated transmembrane protein 4 beta (*LAPTM4B*), phosphatidylinositol glycan anchor biosynthesis class V (*PIGV*) and ankyrin repeat and KH domain containing 1 (*ANKHD1*). It was then hypothesized that the targeted knock out of *LAPTM4B*, *ANKHD1* or *PIGV* in zebrafish produces morphological and functional changes resembling a DCM-like disease state.

The zebrafish (*Danio rerio*) vertebrate animal model was chosen since it provides a quick and easy genetic screening method to assess whether

these genes play a role in DCM development on both a morphological and functional level. Since the basic organ pattern is conserved among vertebrates and zebrafish develop a beating heart within 24 hours post fertilization, they are a valuable model for cardiogenetic studies (18, 19). Zebrafish are not a perfect cardiac model, since structurally they have a two-chamber heart, lacking pulmonary circulation. However, their heart is more similar to the human heart when looking at electrophysiology (heart rate (HR)), action potential duration and morphology. Furthermore, zebrafish embryos are not dependent on their blood circulation until 7 days post fertilization (dpf), enabling functional studies of severe cardiac phenotypes that are otherwise fatal in mammalian models (20). Zebrafish embryos also develop quickly, fully external and are translucent, making manipulation and visualization of the heart using microscopy easier (18). Zebrafish also serve as a good genetic model organism, since the genome is fully sequenced and around 70% of human genes have at least one ortholog in zebrafish (21). In addition, zebrafish are more practical, since they are small and relatively easy and cheap to house. Lastly, their high fecundity, producing approximately 200 eggs per mating, allows them to be used as a rapid screening tool (18).

The three genes of interest (*LAPTM4B, PIGV, ANKHD1*) are all expressed in the heart and possess an ortholog in the zebrafish genome, making them good candidates for further research (22-27). To date, no direct connection has been established between these genes and DCM, underscoring the novelty of this research.

The human *LAPTM4B* gene is located on position 8q22.1 and comprises seven exons (23). The LAPTM4B protein has two known isoforms and plays a role in many processes including endosome transport and regulation of lysosomal membrane permeability. It is localized in several cellular components including the endosome, lysosomal membrane and plasma membrane (23, 28). Within the lysosomal membrane, LAPTM4B contributes to mTORC1 activation via interaction with v-ATPase. More precisely, LAPTM4B recruits the LAT1-4F2hc leucine transporter, enabling leucine uptake and mTORC1 activation via the inside-out mechanism of amino acid sensing (Fig. 2A) (29). It has been shown that the v-ATPase – mTORC1 axis in combination with essential amino acids, plays an important role in preserving the contractile function of cardiomyocytes, suggesting a link between *LAPTM4B* and cardiac function (30, 31). *LAPTM4B* has also been implicated in mucolipidosis type IV (MLIV), a lysosomal storage disorder (LSD). Depletion of LAPTM4B was shown to result in accumulation of electron-dense materials and concentric multilaminar organelles, as is seen in MLIV patients. Thus, *LAPTM4B* shows to be necessary for adequate lysosomal functioning (32). Given that LSDs are associated with cardiac abnormalities, this further implicates LAPTM4B in cardiac pathology (33). Additionally, *LAPTM4B* has been studied in direct relation to the heart. In a study looking at myocardial ischemia/reperfusion (I/R) injury in mice, *LAPTM4B* downregulation exacerbated I/R injury and hypoxia/reoxygenation injury in cardiomyocytes. These effects were attributed to impaired mTORC1 activation, highlighting the critical role of LAPTM4B in regulating autophagic flux during myocardial I/R injury (34). Lastly, *LAPTM4B* exhibits ceramide-binding activity, which also may influence cardiac function, as elevated cardiac levels of total ceramides are seen in heart failure (35). LAPTM4B interacts directly with ceramides and provides a possible 2nd route of late endosome ceramide removal, through export to the extracellular space (Fig. 2A) (36). This ceramide removal route could be a potential link to cardiac dysfunction, since C16:0/C24:0 plasma ceramide levels are directly associated with preclinical LV systolic dysfunction. Elevated ceramides can induce myocardial apoptosis, damage mitochondria, recruit and activate neutrophils, and depress cardiac contractility through dysregulation of calcium influx and cardiac potassium channels (Fig. 2A) (35). Collectively, these studies provide compelling evidence for a potential role of *LAPTM4B* in heart diseases like DCM. The *laptm4b* zebrafish ortholog is localized on chromosome 19, consists of seven exons and encodes a protein localized to lysosomes, endosomes, and the plasma membrane (22, 37).

The human *PIGV* gene is located on position 1p36.11 and comprises six exons (26). *PIGV* has multiple transcript variants, resulting in 10 protein isoforms with differing lengths. The reference protein consists of 493aa and is localized to the endoplasmic reticulum (ER) membrane (26, 38).

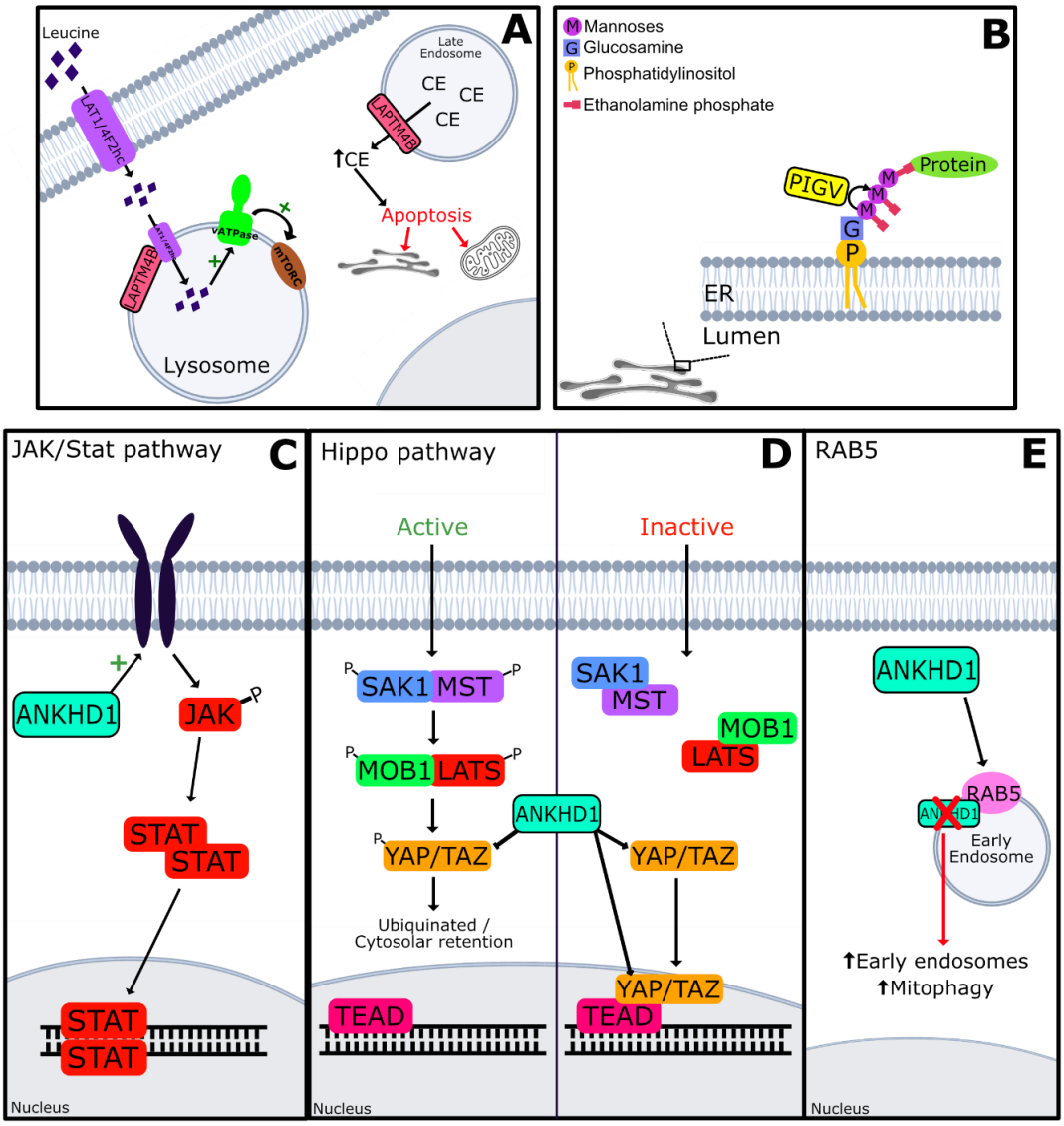

Figure 2 – Function of LAPTM4B, ANKHD1 and PIGV in the cell. ***(A)*** *LAPTM4B localizes to the lysosomal membrane (left), where it recruits the LAT1-4F2hc leucine transporter, enabling leucine uptake. This activates v-ATPase, which subsequently activates the mTORC1 complex. In the late endosomes (right), LAPTM4B interacts directly with ceramides, providing a possible route of ceramide removal. Increased ceramide plasma levels can lead to mitochondrial and endoplasmic reticulum (ER) stress and apoptosis.* ***(B)*** *PIGV catalyzes the addition of the second mannose during the GPI anchor biosynthesis in the ER.* ***(C)*** *The Jak/Stat pathway is initiated through ligand binding which induces JAK receptor dimerization and autophosphorylation, causing STAT dimerization, which affects gene transcription. ANKHD1 enhances receptor levels and thus increases downstream Jak autophosphorylation.* ***(D)*** *The Hippo pathway negatively influences gene transcription. When activated, different complexes are phosphorylated, including YAP/TAZ, which are then ubiquitinated or retained in the cytoplasm. If the pathway is not activated, the YAP/TAZ complex can enter the nucleus where it binds with TEAD and activates gene transcription. ANKHD1 is important in translocation and stabilization of YAP1 and acts as a negative regulator of phosphorylated YAP1.* ***(E)*** *ANKHD1 colocalizes with Rab5 on early endosomes. Knockdown of ANKHD1 increases early endosomes abundance and mitophagy. CE, ceramide; ER, endoplasmic reticulum; GPI, glycosylphosphatidylinositol; JAK, Janus kinase; STAT, signal transducer and activator of transcription; YAP, Yes-associated protein; TAZ, transcriptional co-activator with PDZ-binding motif; TEAD, TEA domain transcription factor; mTORC1, mechanistic target of rapamycin complex 1; LAPTM4B, lysosomal-associated transmembrane protein 4 beta; ANKHD1, ankyrin repeat and KH domain containing 1; PIGV, phosphatidylinositol glycan anchor biosynthesis class V.*

PIGV encodes a mannosyltransferase enzyme involved in the biosynthesis of glycosylphosphatidylinositol (GPI), a membrane anchor for proteins which plays a role in protein sorting and signal transduction pathways (26). The GPI anchor is composed of a phosphatidylinositol (PI) molecule and a glycan core consisting of glucosamine, three mannoses, and an ethanolamine phosphate (36). The entire GPI-AP biosynthetic pathway consists of three major stages: (1) biosynthesis of the GPI anchor, (2) attachment of a protein, and (3) remodeling of the GPI-AP complex. PIGV, also known as GPI-mannosyltransferase II, catalyzes the addition of the second mannose during the GPI anchor biosynthesis (Fig. 2B) (39, 40). *PIGV* mutations have been identified in patients diagnosed with hyperphosphatasia with mental retardation syndrome, otherwise known as Mabry syndrome (41). Patients with this syndrome also present with cardiac phenotypes like atrial septal defects and hypoplastic left heart (41, 42). These findings underscore the potential role for *PIGV* in heart conditions like DCM. The *pigv* zebrafish ortholog is located on chromosome 16, which has three exons (27).

The human *ANKHD1* gene is located on position 5q31.3 and comprises 35 exons (25, 43). The ANKHD1 protein is localized in the cytoplasm and consists of 25 ankyrin motifs grouped into two domains, as well as a single K-homology (KH) domain (43, 44). To date, 22 identified isoforms of ANKHD1 have been identified, with isoform 1 representing the full-length protein (44). *ANKHD1* involved in many well-known signaling pathways, including the JAK/Stat and the Hippo pathway. In the JAK/Stat pathway, ligand binding induces receptor dimerization and autophosphorylation of JAK, leading to phosphorylation and dimerization of STAT, which then translocates to the nucleus, affecting gene transcription. ANKHD1 has been shown to regulate cytokine receptor signaling, allowing for an increase in receptor levels and thus an increase in downstream JAK autophosphorylation (Fig. 2C) (44). The Hippo pathway acts as a negative regulator of gene transcription. Upon activation, different complexes are phosphorylated, including YAP/TAZ, which are then ubiquitinated or retained in the cytoplasm. If the pathway is not activated, the YAP/TAZ complex can enter the nucleus where it binds with TEAD and activates transcription of genes related to proliferation, migration and cellular survival. ANKHD1 plays a dual role in this pathway, by facilitating translocation and stabilization of YAP1, while also acting as a negative regulator of its phosphorylated form (Fig. 2D) (44, 45). ANKDH1 and its effects on these pathways has been mainly implicated in cancer. ANKHD1 has also been shown to contribute in early endosome enlargement, primarily through the colocalization of its ankyrin repeat domains with Rab5. *ANKHD1* knockdown showed an increase in early endosomes, due to decreased membrane vesiculation. This knockdown also lead to a reduction in the number of mitochondria (Fig. 2E) (46). This could be due to mitophagy, since another study that depleted the Drosophila ortholog of *ANKHD1* called Mask, saw an increase in mitophagy (47). The *ankhd1* zebrafish ortholog is localized on chromosome 21 and has 35 exons (24).

In this study, the genetic variants in patients were described and patient data was analyzed to further assess their clinical presentation. These clinical findings were then compared with phenotypes seen in zebrafish knockouts. Functional knockouts of *laptm4b*, *ankhd1* and *pigv* in zebrafish were created using the F0 screening technique, which is an innovative, reverse genetic technique based on CRISPR/Cas9. This method uses three distinct guide RNA (gRNA):Cas9 complexes, targeting different loci within the same gene, ensuring a 90% chance of biallelic knockout in the F0 generation. Unlike traditional stable knockout lines, which take around six months to establish, this technique creates functional knockouts in a matter of days. This makes it a quick and reliable strategy to create knockouts and identify phenotypic changes (48). Knockouts were validated via high resolution melting curve analysis (HRM) to ensure a genotypic change had occurred. The zebrafish embryos were characterized at 3dpf using brightfield microscopy, assessing morphological features (grade of pericardial edema), ventricle size (EDV, ESV, EDA, ESA), and heart function (HR, CO, EF, …) (20). These parameters were obtained through the analyses of short videos of the embryonic heart.

2. EXPERIMENTAL PROCEDURES

2.1 Patient Data – Clinical data was obtained from patients with genetic variants in *LAPTM4B*, *PIGV*, or *ANKHD1*, in the WES study from MUMC+, conducted between 2018 and 2022. Data was provided by MUMC+ and pseudonymized to protect patient privacy. All patients provided written informed consent for use of their data.

2.2 Zebrafish husbandry – Zebrafish of the AB wild-type strain were bred in-house and maintained in a recirculating system under a 14/10 light-dark routine. Embryos were raised in E3 medium, at 28°C. All animal experiments complied with European animal experimentation guidelines and the regulations set by Maastricht University on animal experimentation. All care and experiments involving zebrafish of 5dpf or older were conducted by licensed personnel.

2.3 F0 Screening – The F0 screening protocol was based on Gagnon *et al.*(49), Talbot and Amacher(50), and Kroll *et al.*(48). Three gRNAs per gene were designed. gRNAs for target sequence (TS) 1 and TS3 from *laptm4b* were designed using CRISPRscan (2024) (51). Remaining gRNAs were designed with CHOPCHOP (version 3) (Table 1) (52). Guide constant oligos and short-guide oligos (containing the target sequence, a GC clamp, T7 promotor, and guide constant overlap sequence; Table S1) were ordered from Biolegio. Oligo stocks (1µM) were PCR-amplified using Taq DNA polymerase (2500 Units; Table S2). PCR products were checked via 2% agarose gel electrophoresis and purified with the InnuPrep PCR pure kit (Analytik Jena AG). Concentration and purity were measured with nanodrop (NanoDrop 2000c, ThermoFisher Scientific) followed by gRNA synthesis with the MEGAshortScript T7 kit (ThermoFisher Scientific). Final gRNA products were purified by adding 115µl MilliQ, 15µl NaOAC (3M, pH 5.2), and 150µl phenol:chloroform:isoamyl (1:1:1), followed by vortexing. The aqueous phase was isolated, mixed with 2 volumes 100% EtOH, and incubated at -80°C overnight. Afterwards, samples were centrifuged at maximum speed for 5 min. at 4°C. The supernatant was discarded and the pellet was resuspended in 20-50µl MilliQ. Lastly, final gRNA concentration was measured with the Qubit Fluorometer (ThermoFisher Scientific), using the Qubit RNA Broad Range Assay Kit (Invitrogen, ThermoFisher Scientific).

2.4 Microinjection –Injection mixes contained 1000ng Cas9 (1mg/ml), 1000ng total gRNA (333ng per target), 1µl of a rhodamine solution (5%), and Danieau buffer (1x) to an end volume of 10µl. Injection mixes thus contained a 1:1 ratio gRNA:Cas9 and were incubated at 37°C for 5min. The injection control mix contained rhodamine (5%) in Danieau buffer (1x) at a 1:10 dilution. gRNAs for thymidylate kinase (*tmpk*) served as a positive control (53). Female and male zebrafish were separated into breeding tanks in a 1:1 ratio overnight. The next day, the zebrafish were put together, eggs were collected and put on a 1.5% agarose injection plate (Fig. S1). Eggs were visualized with the M60 stereoscope (Leica microsystems) and injected in the yolk, with 1nl of injection mix, within the first 30min. after fertilization before the first cell division occurred. Injected and non-injected control (NIC) eggs of each clutch were cultured in E3 medium. Three independent injections were performed, resulting in two biological replicates per gene. Approximately

Table 1 – Guide RNA target sequences of laptm4b, pigv and ankhd1.

Gene	*Target Sequence (5'-3')*	*Strand*
laptm4b TS1 (Exon 3)	AGAGGAGCACTGCTAGTACT	+
laptm4b TS2 (Exon 4)	GGTTTACCCCAATACCATAC	-
laptm4b TS3 (Exon 5)	GATAGTCCTGTATGGTATTG	+
pigv TS1 (Exon 2)	AGTTGGGTATCTGCTTCCAC	-
pigv TS2 (Exon 2)	TGGCCGGTTAATCATAACTG	+
pigv TS3 (Exon 2)	CTCTTACTTTTGCAGGCCTC	+
ankhd1 TS1 (Exon 3)	GTTACGCCGGCTGACGTCGT	-
ankhd1 TS2 (Exon 4)	CGTCAACGAGCACACAGAGG	-
ankhd1 TS3 (Exon 5)	GTCAAACTGCTCTTAGTGCA	-

150 eggs were injected per condition per injection. At 1dpf, injected eggs were assessed with a fluorescence microscope (Axiovert 35M, Zeiss). Dead eggs, incompletely stained eggs and completely stained eggs were counted to determine the injection efficiency. Dead or incompletely injected eggs were discarded.

2.5 Phenotypic characterization – At 3dpf, embryos were visualized with the eclipse TS100 inverted phase contrast microscope (Nikon) and categorized based on phenotype: normal, in chorion, mild/moderate pericardial edema, severe pericardial edema, or severe malformations. Phenotypic proportions were quantified by counting embryos in each category. Representative images were captured at 4x magnification using the MicroCam II 20MP camera (Bresser). Heart functionality and ventricle size were assessed at 3dpf via 10-second heart videos. Embryos were anaesthetized with MS222 (0.168 mg/ml) for 2 minutes and put on a specialized imaging agarose gel to ensure a constant sagittal position. The agarose mold is made using a custom 3D printed mold, with thanks to the MERLN research group (Fig. S1). Videos were made at 10x magnification with the eclipse TS100 inverted phase contrast microscope (Nikon) and the MicroCam II 20MP camera (Bresser), ensuring a frame rate of 30 fps. The videos were analyzed with ImageJ (v1.54g). Ventricle size was assessed by end diastolic/systolic area (EDA, ESA) and end diastolic/systolic volume (EDV, ESV). Heart functionality was assessed through heart rate (HR), cardiac output (CO), stroke volume (SV), ejection fraction (EF), relaxation time (RT), contraction time (CT), and fractional area change (FAC). Measurements were taken from three consecutive heartbeats. HR was calculated by determining the fast Fourier transformation (FFT) from the ventricular area (Fig. S2A-B) and using Formula 1. EDA, ESA, the short diameter (Ds), and the long diameter (Dl) were measured at end diastolic and end systolic of three consecutive heartbeats by manually tracing the ventricle (Fig. S2C-E). Derived parameters were calculated using formula 2-6 (54). CT and RT were calculated by determining the frame number at which diastole and systole occurred and using Formula 7 & 8.

$$HR\ (bpm) = \frac{60}{FFT * \frac{1}{fps}} \qquad \textit{Formula 1}$$

$$EDV\ or\ ESV\ (nl) = \frac{\frac{1}{6} * \pi * D_l * D_s^2}{1 * 10^6} \qquad \textit{Formula 2}$$

$$FAC(\%) = 100 * \frac{EDA - ESA}{EDA} \qquad \textit{Formula 3}$$

$$\text{SV (nl/beat)} = \text{EDV} - \text{ESV} \qquad \textit{Formula 4}$$

$$\text{EF(\%)} = (\text{SV/EDV}) * 100 \qquad \textit{Formula 5}$$

$$\text{CO (nl/min)} = \text{SV} * \text{HR} \qquad \textit{Formula 6}$$

$$CT\ (s) = \frac{Frame\ systolic - Frame\ diastolic}{30\ f/s} \qquad \textit{Formula 7}$$

$$RT\ (s) = \frac{Frame\ diastolic - Frame\ systolic}{30\ f/s} \qquad \textit{Formula 8}$$

2.6 High resolution melting curve analysis (HRM) – Following phenotypic characterization, 8 embryos per phenotypic category and per gene were collected for HRM, along with 4 NIC embryos. DNA was extracted by incubating the embryos with proteinase K in SZL-buffer (1:100) for 60min. at 60°C and 15min. at 95°C. DNA extractions were loaded on a 384-multiwell plate in Duplo. HRM was performed using the LightCycler480 HRM master kit (Roche) according to the manufacturer's instructions. Melting curves were obtained with the LightCycler480 instrument (Roche, Table S3) and analyzed with the LightCycler480 Gene scanning software (version 1.5.1). HRM primers (Biolegio) were designed with Primer3Plus (v3.3.0) (Table S4). No suitable primers could be designed for TS1 of *laptm4b*, TS3 of *pigv*, and TS1 of *ankhd1.*

2.7 Statistics – Parameters of each genetic knockout were compared to the NICs. Normality was assessed with the Shapiro-Wilk test and equality of variances was tested with the Brown-Forsythe test. If both were reached an unpaired t-test was performed, if there was no equality of variances a Welch's t-test was performed, and lastly, if there was no normality a Wilcoxon Rank sum test was performed. P-values were adjusted for multiple comparisons using the Bonferroni correction. NIC data from the separate injections were compared with One-way Anova or a Kruskal-Wallis test (if normality was not reached). Phenotypic proportions were analyzed using the Fisher's exact test; Pearson's residuals were calculated when significant. P-values <0.05 were considered statistically significant. All analyses were performed in R studio (v2024.12.1). Detailed

statistical results are presented in Table S5 and Table S6.

3. RESULTS

3.1 Observation of clinical phenotype in patients – Analysis of WES data from 178 idiopathic DCM patients led to the identification of three unique variants in three genes (*LAPTM4B, PIGV, ANKHD1)* (Fig. 1). No additional variants were detected in these genes. Seven patients were identified to have one of these three variants. Their clinical profile were analyzed to gain further insight into the role of these genes in DCM.

3.1.1 LAPTM4B **–** A heterozygous frameshift variant in *LAPTM4B* was identified in three patients. This specific variant involves an insertion of 15 amino acids at position 162 (p.N162insNMCIAIAISLLMIL*), leading to a premature stop codon halfway through the protein sequence. This *LAPTM4B* variant was found in one female patient and two male patients. The average age at diagnosis was 54.6 years, the youngest among the three gene groups. At least one patient had a history of diabetes mellitus, cancer, hypertension and/or hypercholesterolemia. Two of the patients also had a history of arrythmias and one had a history of ischemic heart disease. None of the patients received an ICD implantation due to primary indication, there was however one patient who had an ICD implantation due to secondary indication. All three patients had a family history of cardiac events, namely first degree relatives who underwent coronary intervention due to myocardial infarction (MI), and one reported a case of SCD within their family. This could potentially point to a hereditary gene pattern, however additional family data is required to corroborate this. These patients had an average left ventricular ejection fraction (LVEF) of 42% in echo and 40.3% in CMR, both mildly abnormal (reference range: female 54-74%, male 52-72%)(55). Their average left ventricular end diastolic diameter (LVEDd) was 60mm, indicating ventricular dilation (reference values: female 37.8-52.2mm; Male 42-58.4mm) (55). The severity of DCM is also reflected in the New York Heart Associations (NYHA) classification of heart failure, with two patients having class II and one patient class I heart failure. Aspecific fibrosis was observed in one patient and sporadic mitral valve insufficiency in all three patients. There were no known external factors that could have caused the disease, only one patient had a history of smoking (Table 2).

3.1.2 PIGV **–** In the *PIGV* gene, a substitution of thymine with cytosine at base pair 439 (c.439C>T) was observed, resulting in the creation of a stop codon and a prematurely terminated protein (p.Q147*). This heterozygous *PIGV* variation (rs185641230) was found in two patients. Both patients were female, with an average age of 64.5 years at time of diagnosis. Both patients showed class II heart failure based on the NYHA classification, and an average LVEF of 18% in echo and 24% in CMR, which are both severely abnormal (references values: female 54-74%)(55). They also have an average LVEDd of 59.5mm, which indicates moderate ventricular dilation (reference values: female 37.8-52.2mm) (55). Both patients exhibited mitral valve insufficiency and one showed late gadolinium enhancement (LGE), which indicates fibrosis, in this case specifically septal fibrosis. One of the patients also presented with pericardial effusion. Both patients had a history of COPD and arrythmias. These rhythm problems were clinically significant, as both patients had primary indication of and underwent ICD implantation. The patients had no family history of cardiac events and had no identifiable external factors that could cause their DCM. However, both are former smokers (Table 2).

3.1.3 ANKHD1 **–** Two idiopathic DCM patients carried the same heterozygous *ANKHD1* variation (rs759195447). This variant causes a deletion of an inframe GAG codon, resulting in the deletion of a glutamic acid at amino acid 1492 (p.E1492del). This *ANKHD1* variation was found in a female and a male patient. Their average age at diagnosis was 57 and in at least one patient a history of diabetes mellitus, hypertension and/or hypercholesterolemia was found. Both patients had a history of arrythmias, additionally one of the patients had an ICD implantation with primary indication and one of the patients had an ablation. The average LVEF seen in these patients was 39% in the echo, and 48.5% in CMR. This is below the normal values, indicating a moderately abnormal LVEF (reference values: female 54%-74%, male 52%-72%) (55). The average LVEDd was 58.5mm, consistent with mild to moderate ventricular

dilation (reference values: female 37.8-52.2mm; male 42-58.4mm) (55). This is also reflected in the NYHA classification of both class I and class II. The patients showed no fibrosis and only one patient had a history with alcohol (Table 2).

Table 2 – Clinical data of patients with a genetic variant in PIGV, ANKHD1 or LAPTM4B.

	LAPTM4B	***PIGV***	***ANKHD1***
Number of patients	3	2	2
Sex			
Female	1	2	1
Male	2	0	1
Age at diagnosis	40-63 (±54.6)	54-75 (±64.5)	56-58 (±57)
Medical History			
Diabetes mellitus	2	0	1
COPD	0	2	0
Cancer	1 (before T0)	0	0
Hypertension	1 (after T0)	0	1 (before T0)
Hypercholesterolemia	1 (after T0)	0	2 (before T0)
Arrhythmia	2	2	2
Ischemia	1	0	0
Family History			
SCD	1	0	0
CMP	0	0	0
Coronary intervention MI	3	0	0
NYHA			
Class I	1	0	1
Class II	2	2	1
External Factors			
Former smoker	1	2	0
Alcohol	0	0	1
Drugs	0	0	0
Follow up			
ICD Primary indication	0	2	1
ICD Secondary indication	1	0	0
Ablation	0	0	1
Echo (TTE)			
LVEF, %	35-47 (±42)	17-19 (±18)	23-55 (±39)
LVEDd, mm	55-64 (±60)	57-62 (±59.5)	56-61 (±58.5)
Mitral valve insufficiency	Sporadic	Sporadic/Moderate	No/Minor
CMR			
LVEF, %	33-50 (±40.3)	17-31 (±24)	37-60 (±48.5)
LGE	1 (Aspecific)	1 (Septal Fibrosis)	0
Pericardial effusion	0	1	0

COPD, chronic obstructive pulmonary disease; T0, time of diagnosis; SCD, sudden cardiac death; CMP, cardiomyopathy; MI, myocardial infarction; NYHA, New York Heart Association; ICD, implantable cardioverter defibrillator; TTE, transthoracic echocardiogram; LVEF, left ventricular ejection fraction; LVEDd, left ventricular end diastolic diameter; CMR, cardiac magnetic resonance imaging; LGE, late gadolinium enhancement.

3.2 Genetic knockout of laptm4b, pigv or ankhd1 in zebrafish leads to pericardial edema – To explore the role of *LAPTM4B*, *PIGV* and *ANKHD1* in heart morphology and function further, knockout (KO) zebrafish embryos were created using the F0 screening technique described by Kroll *et al.*(48). Briefly, zebrafish eggs were injected with three different gRNA targets per gene, to ensure a full KO of the gene in the F0 generation. Injection efficiency was assessed at 1dpf, to determine which embryos were successfully injected. An injection control, containing only a rhodamine dye, was also included to observe the effects of the injection itself (Fig. 3A). Approximately 40-50% of the embryos in the KO groups died. Around 20% can be attributed to egg quality, as observed in the NICs. The remaining 20-30% can be attributed to the injection itself. There was no great increase in dead embryos when comparing the injection control with the KO groups, showing that injection with three gRNAs did not greatly effect the mortality of the embryos. Approximately 85% of the viable eggs (~50% of total eggs) were stained by the rhodamine dye and thus successfully injected (Fig. 3B).

The successfully injected eggs were kept in E3 medium and at 3dpf they were phenotyped. The *laptm4b* KOs showed embryos with mild pericardial edema and embryos with severe malformations (Fig. 4A-C). The proportions of the phenotypes were significantly different compared to the NICs, largely due to the increase in embryos with mild pericardial edema and embryos with severe malformations (Fig. 4J & Fig. S7). The *pigv* KOs displayed mild and severe pericardial edema and some embryos with severe malformations. Notably, blood accumulation near the abdomen was frequently observed, indicating circulation defects (Fig. 4D-F). The proportion of phenotypes was significantly different from the NICs, primarily due to the increase in mild pericardial edema, severe pericardial edema and severe malformations (Fig. 4J & Table S6). Lastly, the *ankhd1* KOs showed moderate pericardial edema, severe pericardial edema and severe malformations (Fig. 4G-I). These embryos also showed blood accumulation near the abdomen, indicating circulation defects (Fig. 4G). Again, the proportions were significantly different from the NICs, driven by increased rates of moderate and severe pericardial edema and severe malformations (Fig. 4J & Table S6).

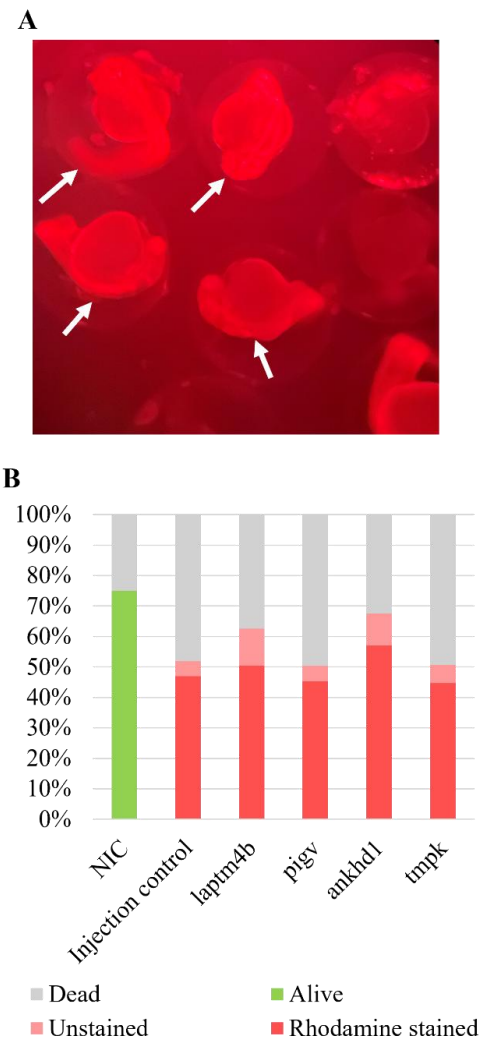

Figure 3 – Average injection efficiency of zebrafish eggs at 1dpf. *Zebrafish eggs were injected with three gRNA targets to ensure full knockout of either laptm4b, pigv, or ankhd1 in the F0 generation. At 1dpf, fluorescence microscopy was used to assess which embryos were stained by the rhodamine dye in the injection mix, and thus which eggs were successfully injected. Dead embryos were counted to assess egg quality and to evaluate the effect of the injection and the CRISPR/Cas9 on mortality rates.* ***(A)*** *Representative image of rhodamine stained embryos. White arrows indicate successfully injected embryos.* ***(B)*** *Phenotypic proportions of the different genetic knockouts. NIC, non-injected control; dpf, days post fertilization; laptm4b, lysosomal-associated transmembrane protein 4 beta; pigv, phosphatidylinositol glycan anchor biosynthesis class V; ankhd1, ankyrin repeat and KH domain containing 1; tmpk, thymidylate kinase.*

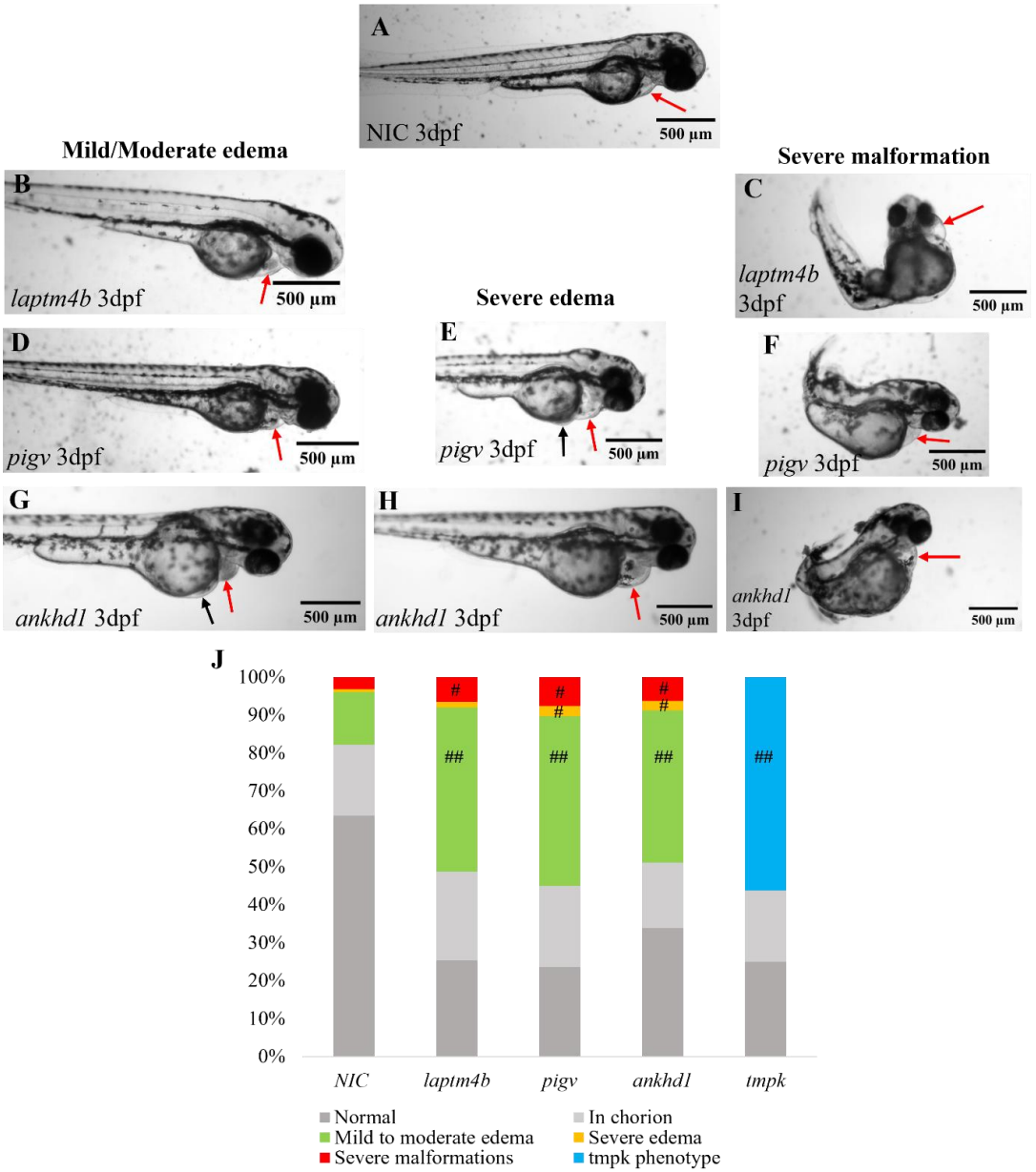

Figure 4 – Genetic knockout of laptm4b, pigv, or ankhd1 leads to morphological changes in zebrafish embryos. *Zebrafish eggs were injected with three gRNA targets to ensure disruption of either laptm4b, pigv, or ankhd1 in the F0 generation. At 3dpf, embryos were imaged and phenotypes were determined and counted. Representative images were taken of these phenotypic groups, red arrows indicate the heart and pericardial area.* ***(A)*** *Non-injected control zebrafish embryo.* ***(B)*** *laptm4b KO embryo showing mild pericardial edema.* ***(C)*** *laptm4b KO embryo showing severe malformations.* ***(D)*** *pigv KO embryo showing mild pericardial edema.* ***(E)*** *pigv KO embryo showing severe pericardial edema and blood accumulation (black arrow).* ***(F)*** *pigv KO embryo showing severe malformations.* ***(G)*** *ankhd1 KO embryo showing moderate pericardial edema and blood accumulation (black arrow).* ***(H)*** *ankhd1 KO embryo showing severe pericardial edema.* ***(I)*** *ankhd1 KO embryo showing severe malformations.* ***(J)*** *Percentual proportions of the different phenotypes seen in the different populations. tmpk serves as a positive control with a known phenotype. Fisher's exact test was used to determine if proportions differed significantly in comparison to the NICs. # Pearson's residuals ≥ 2 ## Pearson's residuals ≥ 10.* ***(J)*** *NIC (n=1026), laptm4b (n=273), pigv (n=327), ankhd1 (n=396), tmpk (n=64). Scale bars are 500µm. NIC, non-injected control; dpf, days post fertilization; KO, knockout; laptm4b, lysosomal-associated transmembrane protein 4 beta; pigv, phosphatidylinositol glycan anchor biosynthesis class V; ankhd1, ankyrin repeat and KH domain containing 1; tmpk, thymidylate kinase.*

In addition to morphological abnormalities, the ventricle size of the KO zebrafish embryos was assessed. At 3dpf, zebrafish embryos were taken randomly, anesthetized for 2min. and 10s videos of the ventricle were captured. End diastolic and systolic area and volume (EDA, EDV, ESA, ESV) were quantified across three consecutive heart beats. There were no significant differences observed in ventricle size between the *laptm4b* KOs and the NICs (Fig. 5). The *pigv* KOs showed no changes in EDV, however they did show a significant decrease in ESV compared to the NICs (Fig. 5A&B). They also showed a significant decrease in both ESA and EDA compared to the NICs (Fig. 5C&D). When analyzing the injections separately, a significant decrease in ESA and ESV could be observed in injection 2 (Fig. S3F&H). However, a decreasing trend can be observed in ESV, EDV, and EDA in the separate injections (Fig. S3E-H). Lastly, the *ankhd1* KOs showed a significant increase in both EDA and ESA compared to the NICs (Fig. 5C&D). No significant changes could be observed in EDV or ESV (Fig. 5A&B). This significant increase was not seen in the separate injections, however a consistent upward trend was observed in EDA and ESA in the separate injections (Fig. S3C-D&G-H). Together, these findings demonstrate that the KO embryos show changes in heart morphology, circulation and ventricle size, and thus that these genes play a role in the morphology of the heart.

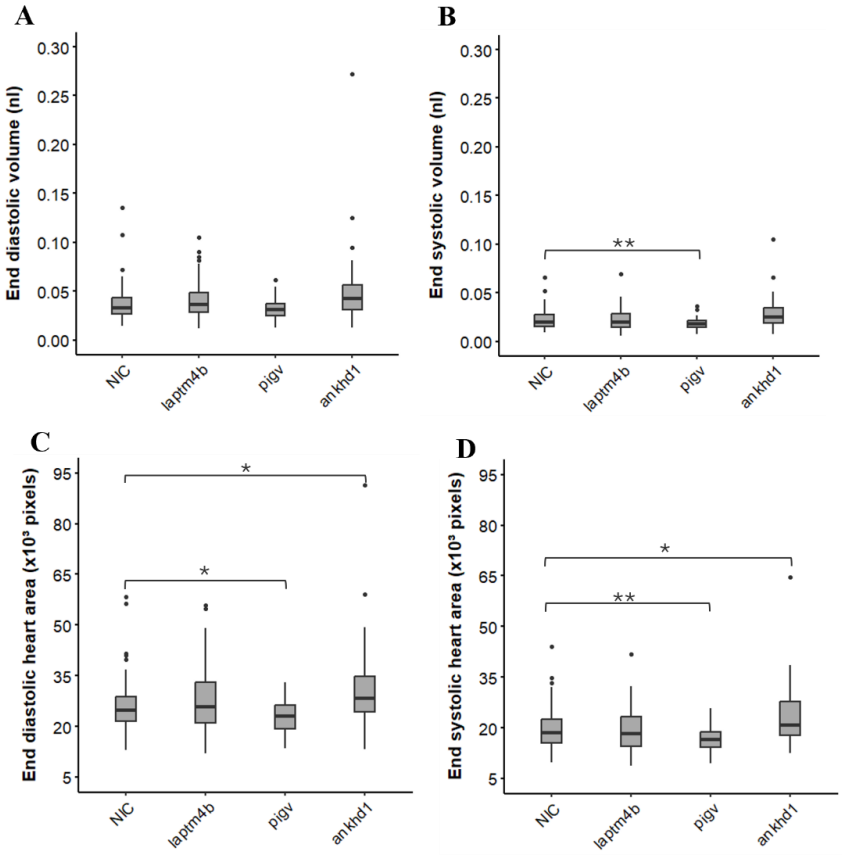

Figure 5 – Ventricle size parameters of genetic knockouts compared to non-injected controls (NIC). *Zebrafish eggs were injected with three gRNA targets to ensure disruption of either laptm4b, pigv, or ankhd1 in the F0 generation. At 3dpf embryos were anesthetized, videos were made of the ventricle to extract ventricle size parameters.* ***(A)*** *End diastolic volume expressed in nanoliters of the different genetic KOs and NICs.* ***(B)*** *End systolic volume expressed in nanoliters of the different genetic KOs and NICs.* ***(C)*** *End diastolic heart area expressed in pixels of the different genetic KOs and NICs.* ***(D)*** *End systolic heart area expressed in pixels of the different genetic KOs and NICs. Data displayed as boxplots showing the median, quartiles and range of values.* ***(A-D)*** *n = 54-64. *p<0.05, **p<0.01. KO, knockout ; laptm4b, lysosomal-associated transmembrane protein 4 beta; pigv, phosphatidylinositol glycan anchor biosynthesis class V ; ankhd1, ankyrin repeat and KH domain containing 1.*

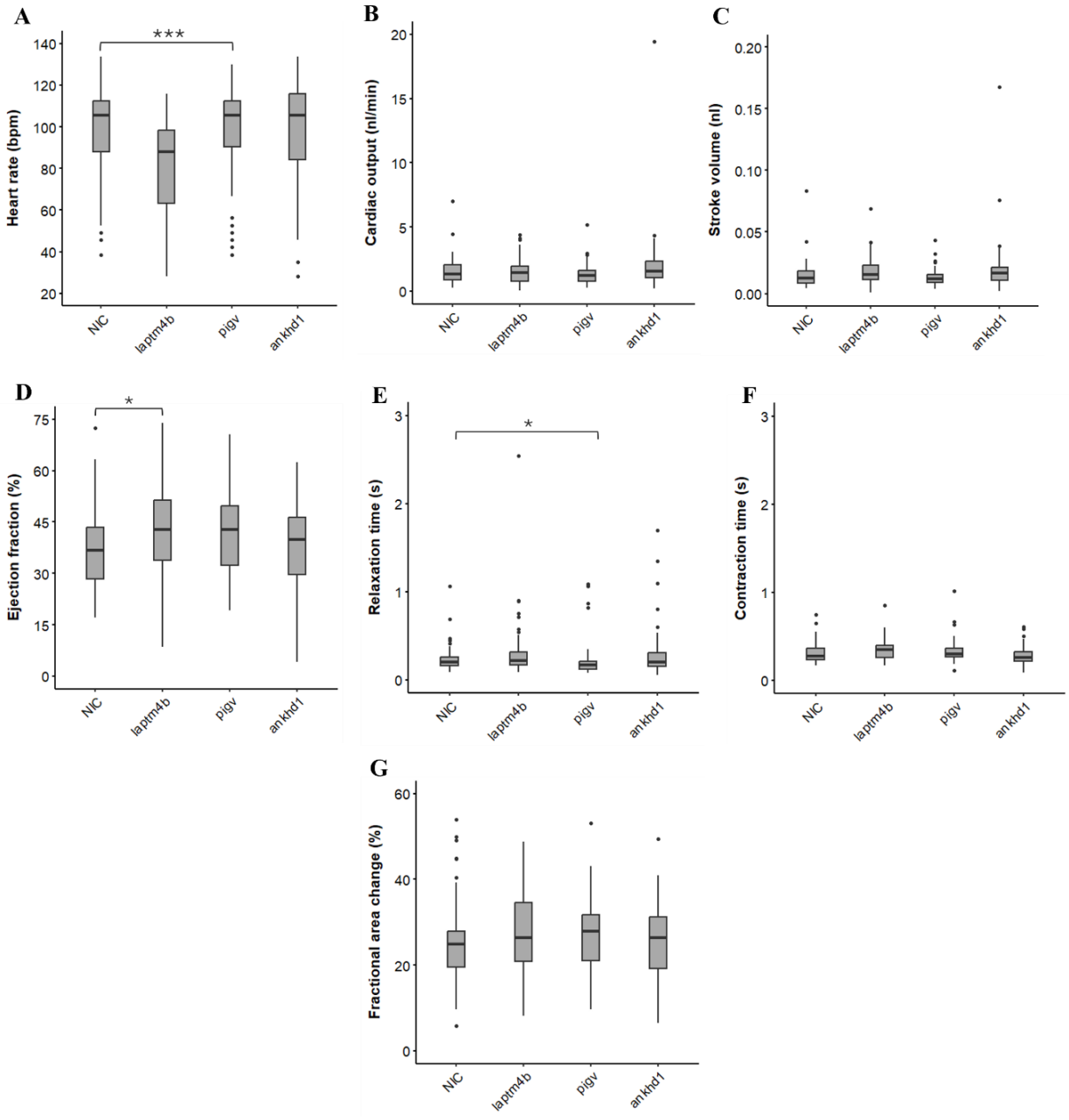

Figure 6 – Heart function parameters of genetic knockouts (KO) compared to the NICs. *Wild type zebrafish eggs were injected with three gRNA targets to ensure disruption of either laptm4b, pigv, or ankhd1 in the F0 generation. At 3dpf embryos were anesthetized and videos were made of the ventricle to extract heart function parameters.* ***(A)*** *Heart rate expressed in beats per minute (bpm) of the different genetic KOs and NICs.* ***(B)*** *Cardiac output expressed in nanoliter per minute (nl/min) of the different genetic KOs and NICs.* ***(C)*** *Stroke volume expressed in nanoliters of the different genetic KOs and NICs.* ***(D)*** *Ejection fraction of the different genetic KOs and NICs.* ***(E)*** *Relaxation time expressed in seconds of the different genetic KOs and NICs.* ***(F)*** *Contraction time expressed in seconds of the different genetic KOs and NICs.* ***(G)*** *Relative contractility measured in the fractional area change of the genetic KOs and NICs.* ***(A)*** *n = 69-83* ***(B-G)*** *n = 54-64. *p<0.05 ***p<0.001. NIC, non-injected control; laptm4b, lysosomal-associated transmembrane protein 4 beta; pigv, phosphatidylinositol glycan anchor biosynthesis class V ; ankhd1, ankyrin repeat and KH domain containing 1.*

3.3 Genetic knockouts of laptm4b, pigv, and ankhd1 show changes in heart function – The heart of the KO embryos was also assessed on a functional level, to determine if these genes play a role in the function of the heart. At 3dpf, zebrafish embryos were taken randomly, anesthetized for 2min. and 10s videos were captured of the ventricle. Functional heart parameters assessed included heart rate (HR), cardiac output (CO), stroke volume (SV), ejection fraction (EF), relaxation time (RT), contraction time (CT), and relative contractility expressed through the fractional area change (FAC). These parameters allowed the evaluation of the dynamic heart function of the KO embryos. In the *laptm4b* KOs there was a significant decrease observed in HR and a significant increase in EF compared to the NICs (Fig. 6A&D). This significant decrease in HR was also observed in injection 3, and a clear downward trend could be seen in injection 1 (Fig. S4A&O). Injection 1 also showed a significant increase in FAC, thus relative contractility, compared to the NICs and in injection 3 there was a significant increase in CT (Fig. S4E&U). An upward trend can also be observed in the CT of the combined injection data (Fig. 6F). The *pigv* KOs showed a significant decrease in RT compared to the NICs, and no other significant changes could be observed (Fig. 6E). When looking at the separate injections, injection 2 shows a significant increase in EF, paired with a significant increase in FAC (Fig. S4K-L). The combined injection follows these findings in an upward trend. Injection 3 also shows a significant increase in CT compared to the NICs (Fig. S4U). Lastly, the *ankhd1* knockouts showed no significant changes in any of the functional heart parameters compared to the NICs (Fig. 6). When looking at the separate injections, there was a significant decrease in CT compared to the NICs in injection 1 (Fig. S4G). These results show that the KO of *laptm4b*, *pigv*, and *ankhd1* affect the functioning of the heart, and thus shows that these genes play a role in maintaining normal heart function.

3.4 Melting curve analysis – To validate the gene knockouts, a HRM analysis was performed using DNA isolated from 3 day old embryos. Melting curves of the different phenotypic groups per genetic KO were compared to see if any genotypic changes had occurred and thus whether the knockout was successful. HRM primers could only be designed for two targets of each gene due to the stringent conditions necessary for HRM. TS1 in *laptm4b* proved to be ineffective since there were no differences in the melting profiles of NICs, embryos with mild edema or embryos with severe malformations. A single duplicate of an embryo showed a deviating profile, however the technical replicate of this embryo still showed a normal pattern, thus this could be due to technical variation (Fig. 7A). No primer could be found for TS2 of *laptm4b* (Fig. 7B), however for TS3 a primer pair could be designed (Fig. 7C). TS3 shows some deviation from the NICs melting profile (Fig. 7C). When comparing the embryos with mild edema and severe malformations with the NICs, there are some clear deviating melting profiles. However there is also some variation in the melting profiles of the NICs as well as in the embryos with mild edema and severe malformations (Fig. 7C-E). For the *pigv* gRNAs, primers could be designed for TS1 and TS2, but not for TS3. When looking at the melting curves for TS1, there is a lot of variation in the melting profile of the NICs, making interpretation of the melting profiles of the embryos with mild edema and severe malformations difficult (Fig. 7F-H). For TS2, there is a more clear melting profile in the NICs. When comparing this to the embryos with a different phenotype, there are embryos with changes in melting curve pattern and embryos with similar melting curves (Fig. 7I-K). Lastly, for *ankhd1* HRM primers could be designed for TS2 and TS3. The melting profile for the NICs of TS2 show some variation making interpretation more difficult (Fig. 7N). When looking at the melting profile of the embryos with mild edema, severe edema, and severe malformations there are some deviations, however most of the embryos follow a similar melting profile as the NICs (Fig. 7P). For TS3, a single embryo with severe malformations showed a deviating melting curve pattern. The other embryos all showed a similar melting profile as the NICs (Fig. 7Q). These results show us that the gRNAs designed for TS1 of *laptm4b*, and TS3 of *ankhd1* prove to be ineffective. However, the gRNAs designed for TS3 of *laptm4b* and TS2 of *pigv* showed to be effective at creating genotypic changes in the injected embryos.

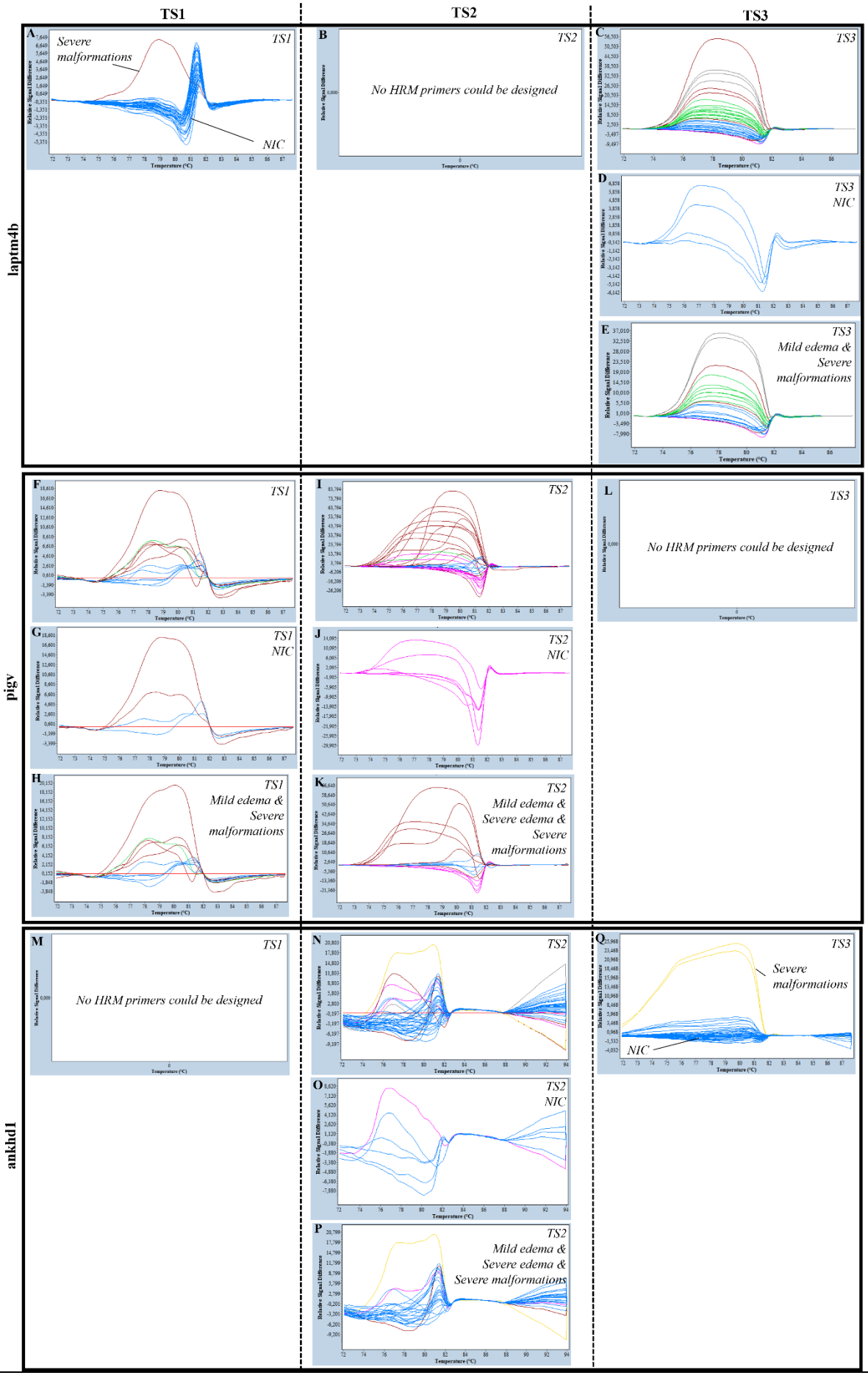
TS1
TS2
TS3
laptm4b
pigy
ankhd1
A
Severe malformations
TS1
NIC
B
TS2
No HRM primers could be designed
C
TS3
D
TS3
NIC
E
TS3
Mild edema & Severe malformations
F
TS1
G
TS1
NIC
H
TS1
Mild edema & Severe malformations
I
TS2
J
TS2
NIC
K
TS2
Mild edema & Severe edema & Severe malformations
L
TS3
No HRM primers could be designed
M
TS1
No HRM primers could be designed
N
TS2
O
TS2
NIC
P
TS2
Mild edema & Severe edema & Severe malformations
Q
TS3
Severe malformations
NIC
Relative Signal Difference
Temperature (°C)

Figure 7 – High resolution melting curve (HRM) analysis of genetic knockouts. *Embryos were collected at 3dpf for DNA isolation. Subsequently, an HRM analysis was done on these samples in Duplo. Normalized and temperature shifted difference plot of* ***(A)*** *Target sequence (TS)1 of laptm4b,* ***(B)*** *TS2 of laptm4b,* ***(C)*** *TS3 of laptm4b,* ***(D)*** *NIC subset from TS3 of laptm4b,* ***(E)*** *mild edema and severe malformation subsets from TS3 of laptm4b,* ***(F)*** *TS1 of pigv,* ***(G)*** *NIC subset from TS1 of pigv,* ***(H)*** *mild edema and severe malformation subsets from TS1 of pigv,* ***(I)*** *TS2 of pigv,* ***(J)*** *NIC subset from TS2 of pigv,* ***(K)*** *mild edema, severe edema and severe malformation subsets from TS2 of pigv,* ***(L)*** *TS3 of pigv,* ***(M)*** *TS1 of ankhd1,* ***(N)*** *TS2 of ankhd1,* ***(O)*** *NIC subset from TS2 of ankhd1,* ***(P)*** *mild edema, severe edema, and severe malformation subsets from TS2 of ankhd1, and* ***(Q)*** *TS3 of ankhd1.* ***(B, L, M)*** *No suitable HRM primers could be designed. Sample sizes per phenotypic group per gene: NIC n = 4; mild edema n = 8; severe edema n = 2; severe phenotype n = 8. laptm4b, lysosomal-associated transmembrane protein 4 beta; pigv, phosphatidylinositol glycan anchor biosynthesis class V; ankhd1, ankyrin repeat and KH domain containing 1; NIC, non-injected control; TS, target sequence.*

4. DISCUSSION

From a cohort of idiopathic DCM patients three potential DCM-causing genes were identified after a stringent filtering process (Fig. 1). It was then hypothesized that the knockout of these genes in zebrafish would cause morphological and functional changes resembling a DCM-like disease state.

4.1 LAPTM4B - LAPTM4B is a transmembrane protein playing a role in mTORC1 activity, ceramide removal, and proper lysosomal functioning, with dysfunction being linked to lysosomal storage disorder MLIV (29, 32, 36). Three idiopathic DCM patients from the cohort showed a frameshift variant in this gene leading to a premature stop codon. These patients were on average 54.6 years of age at diagnosis and had no known external factors that could underly their DCM diagnosis. When looking at the family history of these patients, one patient had a family member with SCD and all three of the patients had first degree family members with coronary interventions due to MI. Thus, there is a pattern of cardiovascular problems within these families. The diagnosis of familial DCM is made when two or more first-degree relatives have "idiopathic" DCM and/or unexplained death at a young age (< 35 years) (6). None of the patients meet these conditions, however this could be due to small family size or variable penetrance of the *LAPTM4B* gene variant. Follow up with the patients and doing sequencing of the first degree relatives could aid in determining the segregation pattern of the *LAPTM4B* gene variation and help in establishing a clear link between gene and disease.

To further explore the role of *LAPTM4B* in DCM, *laptm4b* KOs were made in zebrafish using three gRNA targets. The gRNAs itself did not affect mortality, since there were an equal amount of deaths in the injection control as the *laptm4b* KOs (Fig. 3B). This is in line with the results of Kroll *et al.*(48), which showed that three gRNAs showed a higher penetrance of genetic KO and no significant increase in mortality. We then assessed both the morphology and the functionality of the embryos hearts at 3dpf. Morphologically, around 40% of the embryos showed mild pericardial edema and around 7% showed severe malformations (Fig. 4A-C&J). There was 1% that showed severe edema, however this was not significantly different from what was observed in the NICs. These morphological changes were not paired with any changes in ventricle size (Fig. 5). Thus, the embryos showed a mild morphological phenotype. This could be the result of having at most 2 out of 3 potentially functional gRNAs, since the HRM results showed that the gRNA designed for TS1 proved ineffective (Fig. 7A) and HRM results of TS3 were inconclusive due to high variation in the melting profiles (Fig. 7C-E). Another possibility could be that a stressor is necessary to see the full extent of the *laptm4b* knockout. This hypothesis is strengthened by looking at Gu *et al.*(34) who created a knockout of *Laptm4b* in mice which, in normal conditions, showed no differences in heart size, heart weight, LVEDV, LVESV or LVEF compared to WT mice. However, once they induced ischemia/reperfusion injury in the myocardium of the KO mice, the heart showed much larger infarct size and more cell death (34). Thus, in normal conditions, *Laptm4b* deficient hearts appear normal or mildly affected, however once a stimulus or injury is induced the full extent of the knockout shows.

When looking at functional parameters, the *laptm4b* knockout zebrafish embryos showed a significant decrease in HR and a significant increase in EF compared to the NICs (Fig. 6A&D). When looking at the separate injections, Injection 1

showed a significant increase in FAC, and Injection 3 showed a significant decrease in HR and increase in CT. These functional changes are not in line with what we expect to see in DCM, namely an increase in ventricle size, a decrease in contractility and a decrease in EF (7). These functional changes observed in the zebrafish embryos are more analogous to changes seen in the compensatory stage of cardiac hypertrophy (56). Hypothetically, concentric hypertrophy of the ventricle might not yet increase the ventricle size, whilst increasing the contractility and subsequently the EF of the heart. To compensate for this increase in EF, the zebrafish heart reduces its HR and CT. To test this hypothesis, zebrafish could be evaluated at a later time point to see whether or not this compensation has failed. Additionally, the introduction of a stressor, like EtOH exposure or mechanical shaking, could help in tipping the heart over the edge and showing the full extent of this phenotype (57). The need for a stressor is also in line with the clinical context, since patients only develop DCM later in life. Although the types of DCM are very strict, there is increasing attention to a renewed model of DCM where genetic mutations interact with environmental stimuli (8). These specific patients also showed significant stressors in their medical history like diabetes, cancer and ischemia (Table 2), which strengthen this hypothesis. There is a marked overlap in disease genes between cardiomyopathies like DCM, hypertrophic cardiomyopathy (HCM), and arrhythmogenic right ventricular cardiomyopathy (58). This could be the reason why the KO of a gene found in DCM patients shows a HCM-like phenotype. Another patient was found with a *LAPTM4B* variant by researchers at the institute of cardiology in Montréal. This patient was diagnosed with arrhythmogenic right ventricular cardiomyopathy, further strengthening the hypothesis that the *LAPTM4B* gene plays a more general role in the development of cardiomyopathies.

4.2 PIGV – PIGV is an enzyme that catalyzes the addition of the second mannose during the GPI anchor biosynthesis in the ER (26, 39, 40). From the idiopathic DCM cohort, two patients showed a heterozygous substitution in the *PIGV* gene, leading to a prematurely terminated protein. The two patients were both female, had arrythmia, and underwent ICD implantation (Table 2). Thus, these patients show a clear arrhythmogenic trait, which could be related to the *PIGV* mutation. The patients had no family history of cardiac issues. They were both former smokers and had COPD, which could serve as triggering events for the development of DCM (Table 2). *pigv* KO embryos were made to explore the role of *pigv* in DCM. Three gRNAs were injected, which did not significantly increase the mortality rate of the embryos. Approximately 50% of the *pigv* injected embryos died, while approximately 47% of the injected controls died (Fig. 3B). The HRM analysis revealed that the gRNA for TS2 was effective in creating a genotypic change in the embryos (Fig. 7I-K). For TS1 there was too much variation in the data to make a conclusion about the effectiveness of the gRNA (Fig. 7F-H). This could be due to technical variation and could be solved by repeating the experiment. This could also be due to ineffective primers or possible SNPs in the genome of the embryos at the location of the primer binding sites. To further elucidate this, the primers should be tested on WT embryos, using differing levels of magnesium chloride in the master mix to make sure the primers are functional. Parental fish should also be genotyped to see whether a SNP is present. Primers for the gRNA of TS3 could not be designed properly (Fig. 7L). Thus, only one gRNA could be properly validated.

At 3dpf, the morphology and heart functionality of the KO embryos were assessed with microscopy. The *pigv* KOs showed 45% mild edema, 3% severe edema, and 8% severe malformations. The embryos also showed blood accumulation in the abdomen which is indicative of circulation defects (Fig. 4D-F&J). These morphological changes were paired with a significant decrease in heart area, both EDA and ESA, and a significant decrease in ESV (Fig. 5). This knockout thus shows a more severe phenotype, which could be due to the importance of the *pigv* enzyme in the biosynthesis of the GPI anchor, which serves as a plasma membrane anchor for at least 150 human proteins (39). Thus, if the synthesis of this GPI anchor is defective, many protein functions will be affected, which could have a more severe effect on the zebrafish and the heart. However, the reduction in ventricle size is unexpected, since DCM is characterized by dilation of the left ventricle, and in later stages, of the other heart compartments too (6, 36). This reduction in

ventricle size could be due to general changes in size of the embryos that were not taken into account. So, a measure of ventricle size normalized against the full size of the embryos would further clarify the exact nature of this change in ventricle size. When looking at the *Pigv*^{b2b2859Clo} mouse model (MGI:5645357), the mice are also smaller in size than WT, confirming the need for size normalized measurements of the heart. These mice also show structural cardiovascular defects, however no known cardiomyopathies.

On a functional level, we saw a significant decrease in RT in the *pigv* KOs (Fig. 6E). This means that the heart is going from a contracted state to a relaxed state quicker than the NICs. This is usually due to a reduced afterload, which is the resistance the heart has to contract against. On a molecular level myocardial relaxation happens with the reduction of bound cross-bridges. This is affected by changes in protein isoforms and post-translational modifications that affect the sarcomere, calcium reuptake, and/or cross-bridge kinetics. Thus, the *pigv* knockout could potentially increase this relaxation time by affecting the GPI anchoring of certain proteins that are involved in these processes (59). When looking at the separate injections, Injection 2 showed a significant increase in both EF and FAC, and injection 3 showed a significant increase in CT compared to the NICs (Fig. S4K-L&U). This means that there is an increase in contractility and that contractions are happening slower. This matches the same hypothesis as with *laptm4b*, where hypertrophy of the ventricle could result in an increase in contractility and subsequently an increase in EF. To compensate for this the heart would slow contractions and subsequently the HR. However, no significant changes or trends can be observed in HR in the *pigv* knockouts (Fig. 6A & S6H&O). These functional changes are inconclusive on how they would contribute to the DCM pathophysiology seen in patients. More research is necessary to fully elucidate the role of this gene in the heart and in the development of DCM.

4.3 ANKHD1 – ANKHD1 plays a role in many important pathways like the JAK/Stat pathway and the YAP/TAZ pathway, and plays a role in endosome enlargement (44-46). Two idiopathic DCM patients were identified with an inframe deletion of a glutamic acid at position 1492 (p.E1492del). Both patients had a history of hypercholesterolemia and one of the patients had a history of hypertension. Both patients had arrythmias, with one of them receiving an ICD implantation. Thus, there is possibly an arrhythmogenic trait correlated with the *ANKHD1* gene. The patients do not have a family history of cardiac malfunction (Table 2). Analogous to *LAPTM4B* and *PIGV,* KO zebrafish embryos were created. The injection of the three gRNAs had no effects on mortality, with on average a lower percentage of embryos dying then in the injection control (Fig. 3B). The effectivity of the gRNAs for TS2 and TS3 were checked with HRM, however for the gRNA targeting TS1 no suitable HRM primers could be designed (Fig. 7M). The HRM primers designed for TS2 showed some deviating melting profiles. However, there is also variation in the NICs, thus making interpretation of the effectivity of this gRNA inconclusive (Fig. 7N-P). HRM for this target should be repeated, since these variations could also be due to a random SNP in the zebrafish genome. Lastly, the gRNA of TS3 showed to be not effective at creating genotypic changes since all but one embryo had the same melting profile as the NICs (Fig. 7Q). Thus, the gRNAs for TS1 and TS2 could potentially have induced genotypic changes, however the function of these gRNAs could not be validated.

Morphology and functional characteristics of the *ankhd1* knockouts were assessed at 3dpf. The *ankhd1* injected embryos showed 40% with moderate edema, 3% with severe edema, and 6% with severe malformations. The embryos also showed blood accumulation in the abdomen, which is indicative of a circulatory defect (Fig. 4G-J). These phenotypic changes were accompanied by a significant increase in both EDA and ESA (Fig. 5C&D). This follows the expectation of an increase in ventricle size seen in DCM. In contrast, there is no significant increase in EDV and ESV (Fig. 5A&B). This size difference could thus also be attributed to possible technical variations in the analysis or changes when going from a 2D measurement (EDA, ESA) to a 3D parameter (EDV, ESV). When looking at the functional parameters there are no significant changes compared to the NICs (Fig. 6). When looking at the injections separately, Injection 1 showed a significant decrease in CT, which indicates the heart is contracting faster. This would follow the

DCM disease pattern, since the increase in ventricle size would increase the preload of the heart and thus a first compensatory mechanism of the heart would be to contract faster. However, this should be paired with an increase in HR, which was not seen in these embryos (Fig. 6A & S6A,H,O). On a functional level these KOs do not show many changes, however they do show a more severe morphological phenotype indicating severe changes in the heart and circulation, with at most two functional gRNAs. Thus, it would be valuable to perform more measurements on these KOs on a functional level to further elucidate which effects are biologically relevant and which are due to technical variance.

4.4 Study design – The three genes of interest were originally selected through careful filtering of WES results of 178 idiopathic DCM patients at Maastricht University Hospital. This is an objectively big cohort, but to detect rare and novel variants it is relatively small. Including more idiopathic DCM patients, from the same or other hospitals could strengthen the finding of these variants and their relevance to DCM, but could also aid in finding new potential candidates using the same filtering protocol. Additionally, looking for the prevalence of these variants in other cardiomyopathy patients like HCM patients could also be beneficial in further solidifying the clinical significance of these variants. Also, by increasing the focus on these specific variants a more detailed family history and genetic screens from first-degree relatives could be included to better understand the segregation pattern of these genes. Lastly, from the original analysis 14 variants found in 12 genes (AGAP6, ANKRD20A1, FAM86B1, FAM86B2, FAM98C, GOLGA8H, GOLGA8O, LUC7L2, MUC16, THNSL1, ZNF749, ZNF880) were excluded since they did not have an orthologue in zebrafish. However, these genes should not be discarded since they could still play a significant role in the DCM pathology.

This study is based on the F0 screening technique described by Kroll *et al.*(48), which uses three gRNA targets. This method can increase the chance of biallelic knockout in the F0 generation to over 90% without significantly affecting mortality rates. However, this method is still dependent on good gRNA design. In this study CRISPRscan was used to design gRNAs, since this gRNA prediction tool was developed using zebrafish data. Still, reaching over 90% of animals displaying a phenotype with predicted gRNA scores remains difficult. Lin *et al.*(60) recently developed a new method combining different tools and algorithms to better predict high-efficiency gRNAs, consistently reaching over 80% penetrance with a single gRNA, and up to 100% with two gRNAs. This method could be used to further optimize the gRNAs being used in the F0 screening process, reducing trial and error with finding functional gRNAs. Another difficulty with the F0 screening method is the HRM validation. It is difficult to find suitable HRM primers, since they need to follow very strict conditions like a short amplicon (100-120bp), and the primers should be at least 10bp from the target itself. Sequencing of the target sequences could provide a solution to this, however this is very costly to do on a larger scale, which is necessary when performing screening experiments. Another way to validate whether genotypic changes occurred could be by looking at the molecular level, whether other expected changes occurred. *LAPTM4B* depletion has been shown to lead to the accumulation of electron-dense material and concentric multilaminar organelles, thus looking at the cell organelles would be a way to validate *laptm4b* knockout at the cellular level (32). *PIGV* has been indicated in hyperphosphatasia mental retardation syndrome, thus looking at alkaline phosphate levels in zebrafish could validate *pigv* knockout (41). Lastly, depletion of the *ANKHD1* orthologue Mask lead to an increase in mitophagy, thus looking at the number of mitochondria in the cells could potentially validate *ankhd1* KO (47).

In this study heart videos were generated and from these both the ventricle size, and the functionality of the heart were determined. The analysis of these videos was done with ImageJ, and included manually tracing ventricles and drawing the long and short diameter. This method is highly subjective and vulnerable to bias. There are other methods available, however these are either costly (e.g. video tracking software of ViewPoint), require paid software (61), or are based on fluorescence imaging which is not compatible with our current video acquisition method (62). Thus, there is a great need for alternatives in zebrafish heart analysis that are both freely available and compatible with brightfield imaging. Another way to reduce bias is to have each video analyzed by at least two

different researchers, however since the analysis is very time consuming, this is not always possible. The limitations of this video analysis method could in part explain the high variability in the data between the different injections and the combined data. Another factor in this variability could be the temperature at which the measurements were made since zebrafish heart rate is effected by the temperature (63). This could be solved by using specialized microscopes with heating plates. Additionally, the anesthetic that was used, MS222, also affects the HR of 3 day old embryos. This effect should be negligible since every embryos was exposed to the anesthetic for an equal amount of time (64). Lastly, discrepancies in the significance levels could be due to the fact that each genetic KO has variability of two separate days, whilst the NICs have variability from three days. When comparing the NICs from the different days, there were some significant differences detected (Fig. S5), thus a day effect could play a role in the ventricle size and functional parameters. This could have mainly affected the decrease in HR seen in *laptm4b* KOs, since the HR in NIC2 is significantly higher than that in NIC1 and NIC3. It could also play a role in the significant increase seen in ESA and EDA of *pigv* KOs, since the ESA and EDA of NIC1 was significantly higher than that of NIC2 and NIC3 (Fig. S5). Repeating the F0 screening experiments and thus increasing sample size and power could aid in reducing this day effect.

4.5 Future perspectives – The genes of interest in this study show promising early results, however additional research is necessary before they can be recognized as disease causing genes. Next steps would include optimizing the F0 screening process for these genes by redesigning gRNAs for *laptm4b, pigv,* and *ankhd1*. Additionally, rescue experiments in these F0 screen knockouts should be performed by co-injecting the eggs with the functional human gene and the human variants that were found to see the full effects of these genes in heart function and cardiomyopathy. Setting up stable gRNA lines for further genetic studies would help further research and validation of these genes. Lastly, looking more closely at the underlying mechanisms by looking at the cellular and molecular level in both zebrafish and cell cultures could help in understanding how exactly these genes aid heart function and DCM development.

5. CONCLUSION

In conclusion, this study provides proof of concept that the genes LAPTM4B, PIGV, and ANKHD1 play a role in the normal functioning of the heart and possibly in the development of cardiomyopathies. laptm4b and pigv KO in zebrafish show indications of a HCM pathology, whilst ankhd1 KO show indications of DCM pathology. However, more research is necessary to optimize the F0 screening protocol and to further elucidate how these genes play a role in the development of cardiomyopathies.

REFERENCES

1. Reichart D, Magnussen C, Zeller T, Blankenberg S. Dilated cardiomyopathy: from epidemiologic to genetic phenotypes: A translational review of current literature. J Intern Med. 2019;286(4):362-72.
2. Japp AG, Gulati A, Cook SA, Cowie MR, Prasad SK. The Diagnosis and Evaluation of Dilated Cardiomyopathy. J Am Coll Cardiol. 2016;67(25):2996-3010.
3. Heymans S, Lakdawala NK, Tschope C, Klingel K. Dilated cardiomyopathy: causes, mechanisms, and current and future treatment approaches. Lancet. 2023;402(10406):998-1011.
4. Merlo M, Cannata A, Gobbo M, Stolfo D, Elliott PM, Sinagra G. Evolving concepts in dilated cardiomyopathy. Eur J Heart Fail. 2018;20(2):228-39.
5. Sullivan RD, Mehta RM, Tripathi R, Reed GL, Gladysheva IP. Renin Activity in Heart Failure with Reduced Systolic Function-New Insights. Int J Mol Sci. 2019;20(13).
6. Peters S, Johnson R, Birch S, Zentner D, Hershberger RE, Fatkin D. Familial Dilated Cardiomyopathy. Heart Lung Circ. 2020;29(4):566-74.
7. Wu XY, Lee YK, Lau YM, Au KW, Tse YL, Ng KM, et al. The Pathogenic Mechanisms of and Novel Therapies for Lamin A/C-Related Dilated Cardiomyopathy Based on Patient-Specific Pluripotent Stem Cell Platforms and Animal Models. Pharmaceuticals (Basel). 2024;17(8).
8. Verdonschot JAJ, Hazebroek MR, Krapels IPC, Henkens M, Raafs A, Wang P, et al. Implications of Genetic Testing in Dilated Cardiomyopathy. Circ Genom Precis Med. 2020;13(5):476-87.

9. Westphal JG, Rigopoulos AG, Bakogiannis C, Ludwig SE, Mavrogeni S, Bigalke B, et al. The MOGE(S) classification for cardiomyopathies: current status and future outlook. Heart Fail Rev. 2017;22(6):743-52.
10. Stroik D, Gregorich ZR, Raza F, Ge Y, Guo W. Titin: roles in cardiac function and diseases. Front Physiol. 2024;15:1385821.
11. Veltrop RJA, Kukk MM, Topouzidou K, Didden L, Muchir A, van Steenbeek FG, et al. From gene to mechanics: a comprehensive insight into the mechanobiology of LMNA mutations in cardiomyopathy. Cell Commun Signal. 2024;22(1):197.
12. Captur G, Arbustini E, Bonne G, Syrris P, Mills K, Wahbi K, et al. Lamin and the heart. Heart. 2018;104(6):468-79.
13. Begay RL, Tharp CA, Martin A, Graw SL, Sinagra G, Miani D, et al. FLNC Gene Splice Mutations Cause Dilated Cardiomyopathy. JACC Basic Transl Sci. 2016;1(5):344-59.
14. Whiffin N, Minikel E, Walsh R, O'Donnell-Luria AH, Karczewski K, Ing AY, et al. Using high-resolution variant frequencies to empower clinical genome interpretation. Genet Med. 2017;19(10):1151-8.
15. Rentzsch P, Witten D, Cooper GM, Shendure J, Kircher M. CADD: predicting the deleteriousness of variants throughout the human genome. Nucleic Acids Res. 2019;47(D1):D886-D94.
16. Pejaver V, Byrne AB, Feng BJ, Pagel KA, Mooney SD, Karchin R, et al. Calibration of computational tools for missense variant pathogenicity classification and ClinGen recommendations for PP3/BP4 criteria. Am J Hum Genet. 2022;109(12):2163-77.
17. Ioannidis NM, Rothstein JH, Pejaver V, Middha S, McDonnell SK, Baheti S, et al. REVEL: An Ensemble Method for Predicting the Pathogenicity of Rare Missense Variants. Am J Hum Genet. 2016;99(4):877-85.
18. Gut P, Reischauer S, Stainier DYR, Arnaout R. Little Fish, Big Data: Zebrafish as a Model for Cardiovascular and Metabolic Disease. Physiol Rev. 2017;97(3):889-938.
19. Kimmel CB, Ballard WW, Kimmel SR, Ullmann B, Schilling TF. Stages of embryonic development of the zebrafish. Dev Dyn. 1995;203(3):253-310.
20. Narumanchi S, Wang H, Perttunen S, Tikkanen I, Lakkisto P, Paavola J. Zebrafish Heart Failure Models. Front Cell Dev Biol. 2021;9:662583.
21. Howe K, Clark MD, Torroja CF, Torrance J, Berthelot C, Muffato M, et al. The zebrafish reference genome sequence and its relationship to the human genome. Nature. 2013;496(7446):498-503.
22. laptm4b lysosomal protein transmembrane 4 beta [Danio rerio (zebrafish)] - Gene - NCBI [2025-01-02]. Available from: https://www.ncbi.nlm.nih.gov/gene/?term=Danio+rerio+laptm4b.
23. LAPTM4B lysosomal protein transmembrane 4 beta [Homo sapiens (human)] - Gene - NCBI [2024-09-30]. Available from: https://www.ncbi.nlm.nih.gov/gene/55353#general-gene-info.
24. ankhd1 ankyrin repeat and KH domain containing 1 [Danio rerio (zebrafish)] - Gene - NCBI [2025-01-02]. Available from: https://www.ncbi.nlm.nih.gov/gene/?term=Danio+rerio+ankhd1.
25. ANKHD1 ankyrin repeat and KH domain containing 1 [Homo sapiens (human)] - Gene - NCBI [2024-10-02]. Available from: https://www.ncbi.nlm.nih.gov/gene/54882#bibliography.
26. PIGV phosphatidylinositol glycan anchor biosynthesis class V [Homo sapiens (human)] - Gene - NCBI [2024-10-02]. Available from: https://www.ncbi.nlm.nih.gov/gene/55650.
27. pigv phosphatidylinositol glycan anchor biosynthesis, class V [Danio rerio (zebrafish)] - Gene - NCBI [2025-01-02]. Available from: https://www.ncbi.nlm.nih.gov/gene/?term=Danio+rerio+pigv.
28. LAPTM4B - Lysosomal-associated transmembrane protein 4B - Homo sapiens (Human) | UniProtKB | UniProt [2024-12-20]. Available from: https://www.uniprot.org/uniprotkb/Q86VI4/entry#sequences.
29. Milkereit R, Persaud A, Vanoaica L, Guetg A, Verrey F, Rotin D. LAPTM4b recruits the LAT1-4F2hc Leu transporter to lysosomes and promotes mTORC1 activation. Nat Commun. 2015;6:7250.
30. Wang S, Han Y, Liu R, Hou M, Neumann D, Zhang J, et al. Glycolysis-Mediated Activation

of v-ATPase by Nicotinamide Mononucleotide Ameliorates Lipid-Induced Cardiomyopathy by Repressing the CD36-TLR4 Axis. Circ Res. 2024;134(5):505-25.
31. Wang S, Schianchi F, Neumann D, Wong LY, Sun A, van Nieuwenhoven FA, et al. Specific amino acid supplementation rescues the heart from lipid overload-induced insulin resistance and contractile dysfunction by targeting the endosomal mTOR-v-ATPase axis. Mol Metab. 2021;53:101293.
32. Vergarajauregui S, Martina JA, Puertollano R. LAPTMs regulate lysosomal function and interact with mucolipin 1: new clues for understanding mucolipidosis type IV. J Cell Sci. 2011;124(Pt 3):459-68.
33. Nair V, Belanger EC, Veinot JP. Lysosomal storage disorders affecting the heart: a review. Cardiovascular Pathology. 2019;39:12-24.
34. Gu S, Tan J, Li Q, Liu S, Ma J, Zheng Y, et al. Downregulation of LAPTM4B Contributes to the Impairment of the Autophagic Flux via Unopposed Activation of mTORC1 Signaling During Myocardial Ischemia/Reperfusion Injury. Circ Res. 2020;127(7):e148-e65.
35. Park LK, Garr Barry V, Hong J, Heebink J, Sah R, Peterson LR. Links between ceramides and cardiac function. Curr Opin Lipidol. 2022;33(1):47-56.
36. Blom T, Li S, Dichlberger A, Back N, Kim YA, Loizides-Mangold U, et al. LAPTM4B facilitates late endosomal ceramide export to control cell death pathways. Nat Chem Biol. 2015;11(10):799-806.
37. laptm4b - Lysosomal-associated transmembrane protein 4B - Danio rerio (Zebrafish) | UniProtKB | UniProt [2025-01-02 11:36:51]. Available from: https://www.uniprot.org/uniprotkb/Q801V1/entry#subcellular_location.
38. PIGV - GPI mannosyltransferase 2 - Homo sapiens (Human) | UniProtKB | UniProt [2024-10-02]. Available from: https://www.uniprot.org/uniprotkb/Q9NUD9/entry#interaction.
39. Wu T, Yin F, Guang S, He F, Yang L, Peng J. The Glycosylphosphatidylinositol biosynthesis pathway in human diseases. Orphanet J Rare Dis. 2020;15(1):129.
40. Kang JY, Hong Y, Ashida H, Shishioh N, Murakami Y, Morita YS, et al. PIG-V involved in transferring the second mannose in glycosylphosphatidylinositol. J Biol Chem. 2005;280(10):9489-97.
41. Horn D, Wieczorek D, Metcalfe K, Baric I, Palezac L, Cuk M, et al. Delineation of PIGV mutation spectrum and associated phenotypes in hyperphosphatasia with mental retardation syndrome. Eur J Hum Genet. 2014;22(6):762-7.
42. Conte F, Sam JE, Lefeber DJ, Passier R. Metabolic Cardiomyopathies and Cardiac Defects in Inherited Disorders of Carbohydrate Metabolism: A Systematic Review. Int J Mol Sci. 2023;24(10).
43. ANKHD1 - Ankyrin repeat and KH domain-containing protein 1 - Homo sapiens (Human) | UniProtKB | UniProt [2024-12-02]. Available from: https://www.uniprot.org/uniprotkb/Q8IWZ3/entry.
44. Mullenger JL, Zeidler MP, Fragiadaki M. Evaluating the Molecular Properties and Function of ANKHD1, and Its Role in Cancer. Int J Mol Sci. 2023;24(16).
45. Almeida BO, Machado-Neto JA. Emerging functions for ANKHD1 in cancer-related signaling pathways and cellular processes. BMB Rep. 2020;53(8):413-8.
46. Kitamata M, Hanawa-Suetsugu K, Maruyama K, Suetsugu S. Membrane-Deformation Ability of ANKHD1 Is Involved in the Early Endosome Enlargement. iScience. 2019;17:101-18.
47. Zhu M, Li X, Tian X, Wu C. Mask loss-of-function rescues mitochondrial impairment and muscle degeneration of Drosophila pink1 and parkin mutants. Hum Mol Genet. 2015;24(11):3272-85.
48. Kroll F, Powell GT, Ghosh M, Gestri G, Antinucci P, Hearn TJ, et al. A simple and effective F0 knockout method for rapid screening of behaviour and other complex phenotypes. Elife. 2021;10.
49. Gagnon JA, Valen E, Thyme SB, Huang P, Akhmetova L, Pauli A, et al. Efficient mutagenesis by Cas9 protein-mediated oligonucleotide insertion and large-scale assessment of single-guide RNAs. PLoS One. 2014;9(5):e98186.
50. Talbot JC, Amacher SL. A streamlined CRISPR pipeline to reliably generate zebrafish frameshifting alleles. Zebrafish. 2014;11(6):583-5.
51. Moreno-Mateos MA, Vejnar CE, Beaudoin JD, Fernandez JP, Mis EK, Khokha MK, et al. CRISPRscan: designing highly efficient sgRNAs

for CRISPR-Cas9 targeting in vivo. Nat Methods. 2015;12(10):982-8.
52. Labun K, Montague TG, Krause M, Torres Cleuren YN, Tjeldnes H, Valen E. CHOPCHOP v3: expanding the CRISPR web toolbox beyond genome editing. Nucleic Acids Res. 2019;47(W1):W171-W4.
53. Vanoevelen JM, Bierau J, Grashorn JC, Lambrichs E, Kamsteeg EJ, Bok LA, et al. DTYMK is essential for genome integrity and neuronal survival. Acta Neuropathol. 2022;143(2):245-62.
54. Yalcin HC, Amindari A, Butcher JT, Althani A, Yacoub M. Heart function and hemodynamic analysis for zebrafish embryos. Dev Dyn. 2017;246(11):868-80.
55. Lang RM, Badano LP, Mor-Avi V, Afilalo J, Armstrong A, Ernande L, et al. Recommendations for cardiac chamber quantification by echocardiography in adults: an update from the American Society of Echocardiography and the European Association of Cardiovascular Imaging. Eur Heart J Cardiovasc Imaging. 2015;16(3):233-70.
56. Bernardo BC, Ooi JYY, McMullen JR. The yin and yang of adaptive and maladaptive processes in heart failure. Drug Discovery Today: Therapeutic Strategies. 2012;9(4):e163-e72.
57. Valcarce DG, Selles-Egea A, Riesco MF, De Garnica MG, Martinez-Fernandez B, Herraez MP, et al. Early stress exposure on zebrafish development: effects on survival, malformations and molecular alterations. Fish Physiol Biochem. 2024;50(4):1545-62.
58. Haas J, Frese KS, Peil B, Kloos W, Keller A, Nietsch R, et al. Atlas of the clinical genetics of human dilated cardiomyopathy. Eur Heart J. 2015;36(18):1123-35a.
59. Chung CS, Hoopes CW, Campbell KS. Myocardial relaxation is accelerated by fast stretch, not reduced afterload. J Mol Cell Cardiol. 2017;103:65-73.
60. Lin SJ, Huang K, Petree C, Qin W, Varshney P, Varshney GK. Optimizing gRNA selection for high-penetrance F0 CRISPR screening for interrogating disease gene function. Nucleic Acids Res. 2025;53(5).
61. Shin JT, Pomerantsev EV, Mably JD, MacRae CA. High-resolution cardiovascular function confirms functional orthology of myocardial contractility pathways in zebrafish. Physiol Genomics. 2010;42(2):300-9.
62. Vedder VL, Reinberger T, Haider SMI, Eichelmann L, Odenthal N, Abdelilah-Seyfried S, et al. pyHeart4Fish: Chamber-specific heart phenotype quantification of zebrafish in high-content screens. Front Cell Dev Biol. 2023;11:1143852.
63. Barrionuevo WR, Burggren WW. O2 consumption and heart rate in developing zebrafish (Danio rerio): influence of temperature and ambient O2. Am J Physiol. 1999;276(2):R505-13.
64. Collymore C, Banks EK, Turner PV. Lidocaine Hydrochloride Compared with MS222 for the Euthanasia of Zebrafish (Danio rerio). J Am Assoc Lab Anim Sci. 2016;55(6):816-20.

Acknowledgements – FJH wants to thank Dr. Jo Vanoevelen and MUMC+ for the opportunity for this internship and to provide the resources to complete this research. Nina Beelen and Dr. J.A.J. Verdonschot are gratefully acknowledged for providing the clinical patient data and to provide their input in the understanding and interpretation of this data. Dr. Dimitris Kapsokalyvas is thanked for assisting with microscopy. FJH wants to acknowledge the MERLN research group for the 3D printed molds they provided. FJH gratefully acknowledges Leela Chatterji for performing the original WES data filtering, which identified the three genes of interest, and for the gRNA design of pigv and ankhd1. Lastly, FJH wants to thank Kevin van Dorsten and Rhestrie Sheombarsing for their support during this internship.

Author contributions – JV and FJH conceived and designed the research. FJH performed experiments and data analysis. EL, JG and JV provided assistance with microinjections and performed animal care. EL and JG provided assistance with HRM experiments and data analysis. FJH wrote the paper. All authors revised and provided feedback on the manuscript.

SUPPLEMENTALS

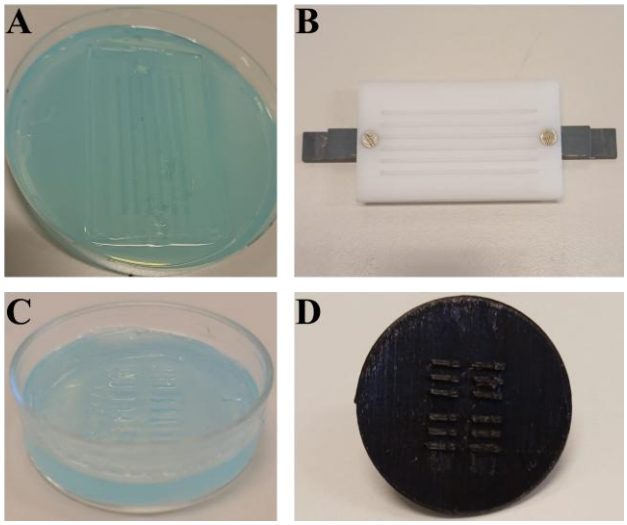

Figure S1 – Agarose gel plates for injection and video acquisition. ***(A)*** *Injection plate made from 1.5% agarose gel in E3 medium. The agarose plate was made using* ***(B)*** *a mold.* ***(C)*** *Video acquisition plates made from a 2% agarose gel in E3 medium. Plate was made using a two-step pour approach, providing support for* ***(D)*** *the 3D printed mold. Plates were stored at 4°C covered in E3 medium to avoid shrinkage. After use, plates were washed with 70% ethanol and distilled water, and reused.*

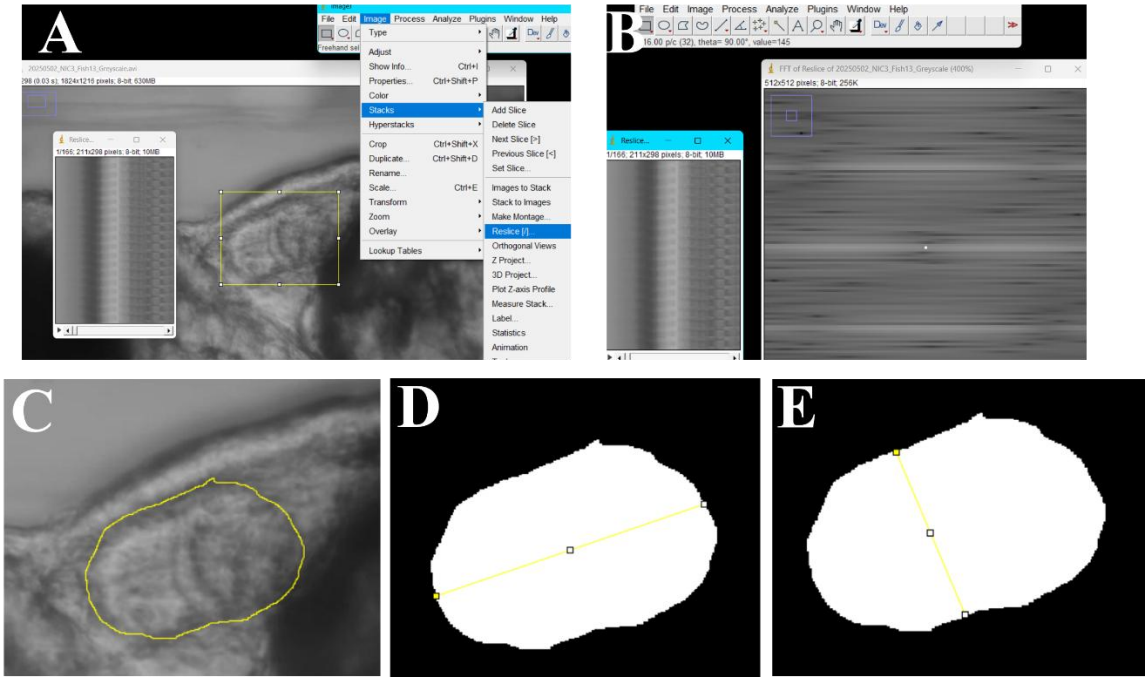

Figure S2 – ImageJ analysis of heart videos. *Heart rate is calculated by determining the FFT by first* ***(A)*** *reslicing the area of the ventricle and next* ***(B)*** *calculating the FFT from a striped section of the resliced image.* ***(C)*** *End systolic and diastolic area is measured by tracing the ventricle and measuring the area.* ***(D-E)*** *The diameter is measured in the mask of the traced ventricle. FFT, fast fourier transformation.*

Table S1 - Guide-constant oligo and short-guide oligos for laptm4b, pigv and ankhd1.

Name	Sequence (5'-3')
laptm4b TS1 (Exon 3)	GCGTAATACGACTCACTATAGGAGAGGAGCACTGCTAGTACTGTTTTAGAGCTAGAAATAGC
laptm4b TS2 (Exon 4)	GCGTAATACGACTCACTATAGGGGTTTACCCCAATACCATACGTTTTAGAGCTAGAAATAGC
laptm4b TS3 (Exon 5)	GCGTAATACGACTCACTATAGGGATAGTCCTGTATGGTATTG GTTTTAGAGCTAGAAATAGC
pigv TS1 (Exon 2)	GCGTAATACGACTCACTATAGGAGTTGGGTATCTGCTTCCACGTTTTAGAGCTAGAAATAGC
pigv TS2 (Exon 2)	GCGTAATACGACTCACTATAGGTGGCCGGTTAATCATAACTGGTTTTAGAGCTAGAAATAGC
pigv TS3 (Exon 2)	GCGTAATACGACTCACTATAGGCTCTTACTTTTGCAGGCCTCGTTTTAGAGCTAGAAATAGC
ankhd1 TS1 (Exon 3)	GCGTAATACGACTCACTATAGGGTTACGCCGGCTGACGTCGTGTTTTAGAGCTAGAAATAGC
ankhd1 TS2 (Exon 4)	GCGTAATACGACTCACTATAGGCGTCAACGAGCACACAGAGGGTTTTAGAGCTAGAAATAGC
ankhd1 TS3 (Exon 5)	GCGTAATACGACTCACTATAGGGTCAAACTGCTCTTAGTGCAGTTTTAGAGCTAGAAATAGC
Guide-constant oligo	AAAGCACCGACTCGGTGCCACTTTTTCAAGTTGATAACGGACTAGCCTTATTTTAACTTGCTATTTCTAGCTCTAAAAC
tmpk TS1 (Exon 2)	GCGTAATACGACTCACTATAGGATAGACAGAACTACTAAGATGTTTTAGAGCTAGAAATAGC
tmpk TS2 (Exon 3)	GCGTAATACGACTCACTATAGGAGGAAGGAATTAATCTAGGTTTTAGAGCTAGAAATAGCAAG
tmpk TS3 (Exon 4)	GCGTAATACGACTCACTATAGGGACTTCCAAAACCAGACCGTTTTAGAGCTAGAAATAGCAAG

GC clamp, T7 promotor, **guide constant overlap**.

Table S2 - Thermocycling conditions of PCR amplification of gRNA template oligos.

	Temperature	Time	Remarks
	95°C	30 seconds	
Amplification	95°C	15 seconds	40 cycles
	60°C	30 seconds	
	72°C	20 seconds	
Final extension	72°C	5 minutes	
Hold	4°C	∞	

Table S3 - Thermocycling conditions for high resolution melting curve analysis.

	Temperature	Time	Remarks
Pre-incubation	95°C	10 minutes	
Amplification	95°C	10 seconds	45 cycles
	59°C	15 seconds	
	72°C	15 seconds	
Melting	60°C → 95°C	0.02°C/s	25 acquisitions/s
Cooling	95°C → 40°C		

Table S4 – HRM primers for different targets sequences of laptm4b, pigv and ankhd1.

Target	Forward Primer (5'-3')	Reverse Primer (5'-3')
laptm4b TS1 (Exon 3)	TGTGTTACCTTGAAAGCTAAGATGCATCCA	ACAGCCTGGGACCTTTCCATACAAA
laptm4b TS3 (Exon 5)	CGTAGGTTGCCATTCCACAAATCAAAATCA	AGGCGCAATATCCCTTACACAAATCTGA
pigv TS1 (Exon 2)	CCATTGGCAGATTCCACTTT	AATCCCAGAGTTGCAACAGG
pigv TS2 (Exon 2)	ATTGCTATGGCCATTGTGTG	CCAGAGGCCTGCAAAAGTAA
ankhd1 TS2 (Exon 4)	AAGCTGCTAGACGAGGGACGCA	ACCTGTGGAGCTCATAGTATCCAGC
ankhd1 TS3 (Exon 5)	GGGATTAAAGGAGACATCACGCCACTAAT	GTTGTACCTGTTGAAGACTGTGCATTAACA

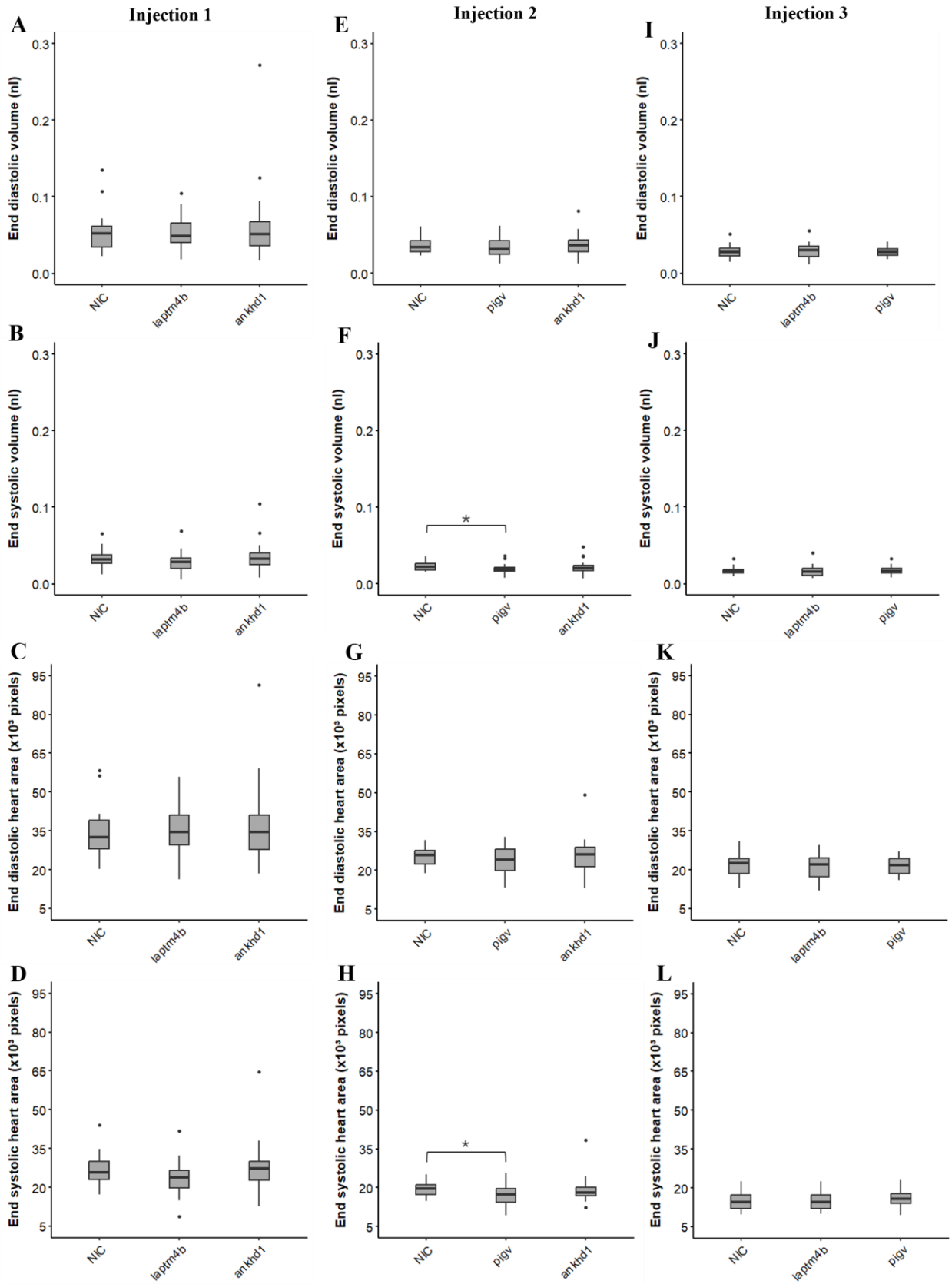
Injection 1
Injection 2
Injection 3
A
B
C
D
E
F
G
H
I
J
K
L
End diastolic volume (nl)
End systolic volume (nl)
End diastolic heart area (x10³ pixels)
End systolic heart area (x10³ pixels)
NIC
laptm4b
pigv
ankhd1
*

Figure S3 – Ventricle size parameters of genetic knockouts compared to non-injected controls (NICs) for each separate injection. *Zebrafish eggs were injected with three gRNA targets to ensure disruption of either laptm4b, pigv, or ankhd1 in the F0 generation. At 3dpf embryos were anesthetized, videos were made of the ventricle to extract ventricle size parameters.* ***(A, D, H)*** *End diastolic volume expressed in nanoliters of the different genetic KOs and NICs.* ***(B, E, I)*** *End systolic volume expressed in nanoliters of the different genetic KOs and NICs.* ***(C, F, J)*** *End diastolic heart are expressed in pixels of the different genetic KOs and NICs.* ***(D, G, .)*** *End systolic heart area expressed in pixels of the different genetic KOs and NICs. Data displayed as boxplots showing the median, quartiles and range of values.* ***(A-D)*** *Injection 1 (n = 18-30).* ***(E-G)*** *Injection 2 (n = 18-32).* ***(H-K)*** *Injection 3 (n = 22-30). *p<0.05. KO, knockout; laptm4b, lysosomal-associated transmembrane protein 4 beta; pigv, phosphatidylinositol glycan anchor biosynthesis class V; ankhd1, ankyrin repeat and KH domain containing 1.*

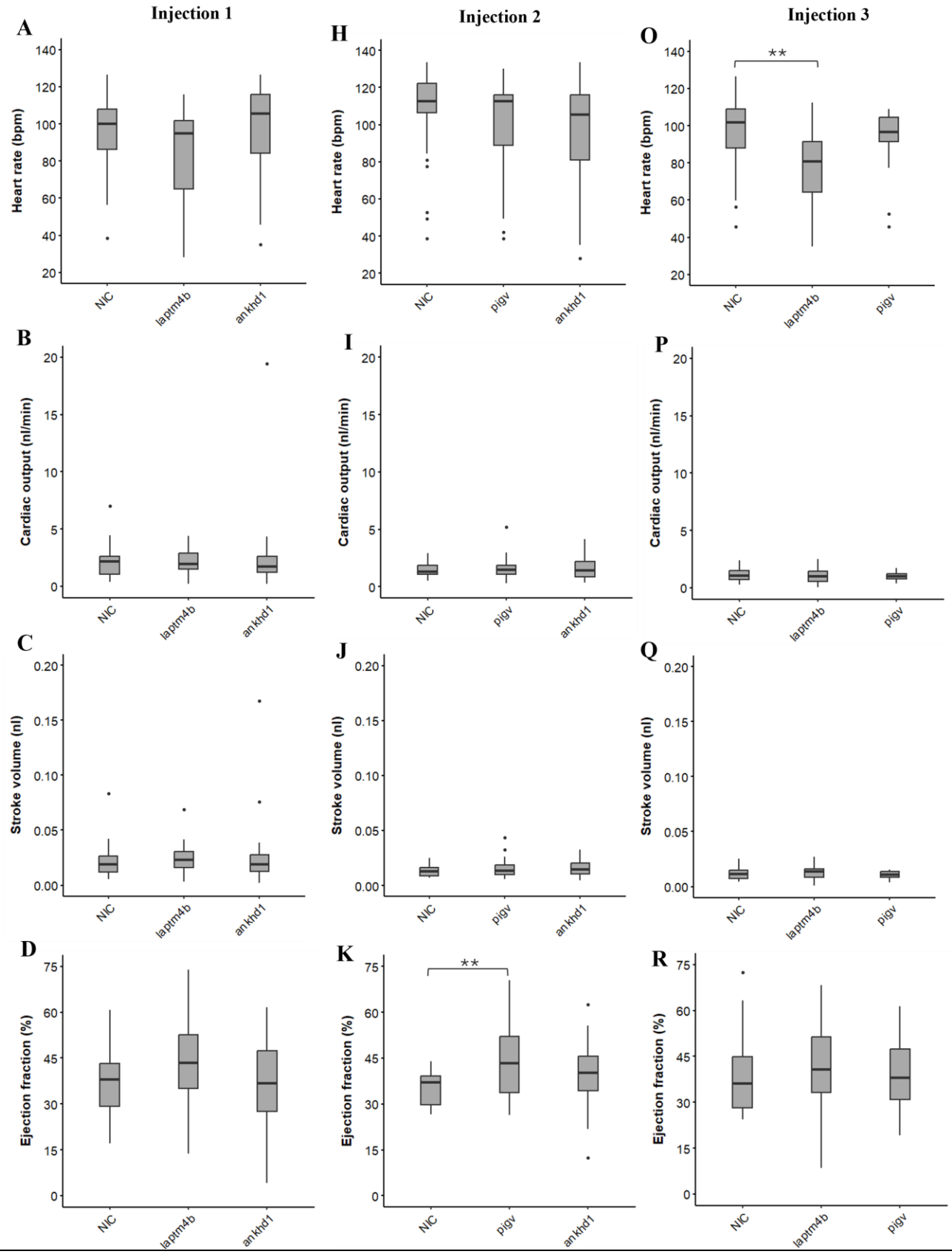
Injection 1
Injection 2
Injection 3
A
H
O
B
I
P
C
J
Q
D
K
R
Heart rate (bpm)
Cardiac output (nl/min)
Stroke volume (nl)
Ejection fraction (%)
**
NIC
laptm4b
pigv
ankhd1

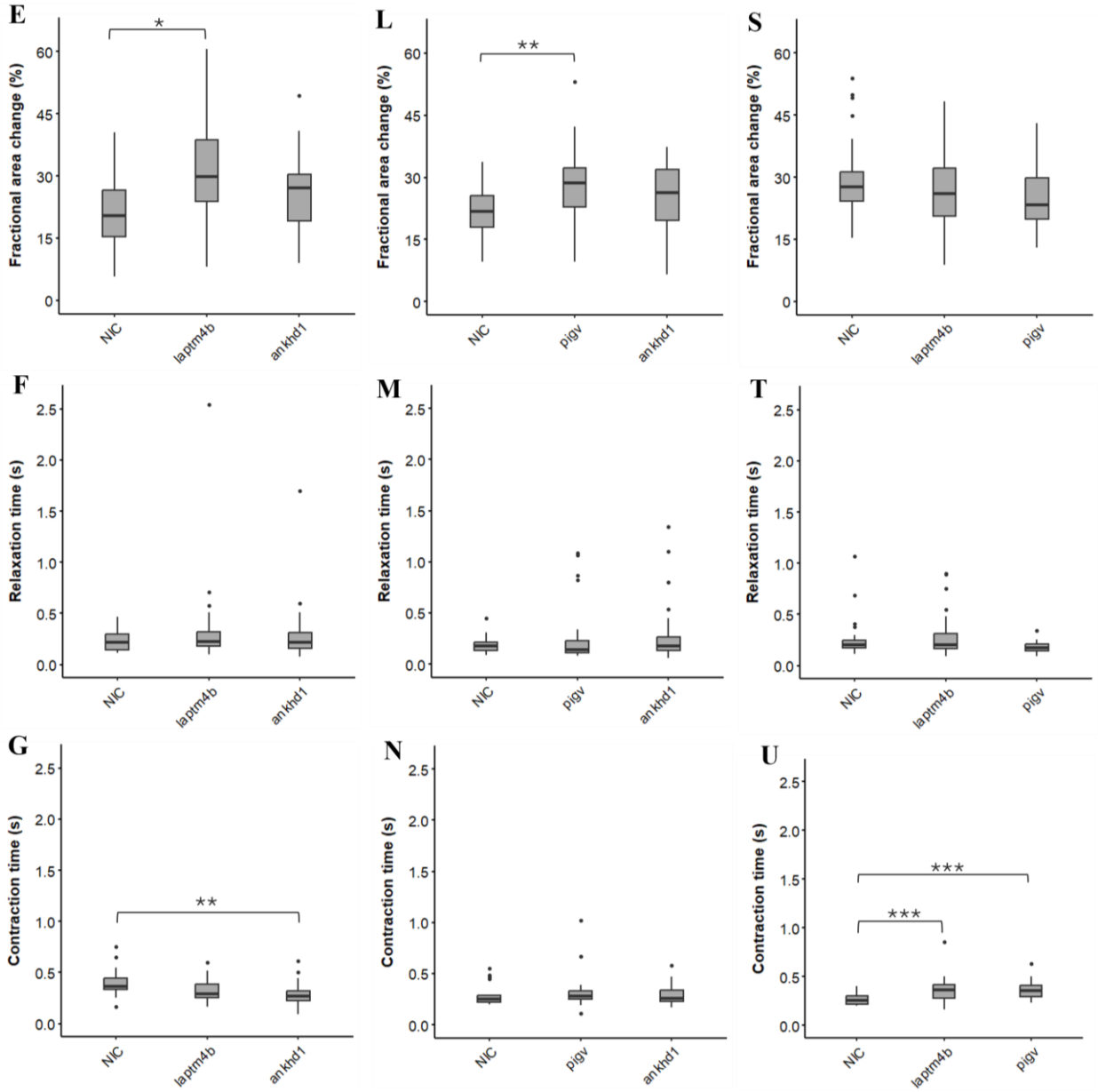

Figure S4 – Heart function parameters of genetic knockouts (KO) compared to non-injected controls (NICs) for each separate injection. *Wild type zebrafish eggs were injected with three gRNA targets to ensure disruption of either laptm4b, pigv, or ankhd1 in the F0 generation. At 3dpf embryos were anesthetized and videos were made of the ventricle to extract heart function parameters.* ***(A, H, O)*** *Heart rate expressed in beats per minute (bpm) of the different genetic KOs and NICs.* ***(B, I, P)*** *Cardiac output expressed in nanoliter per minute (nl/min) of the different genetic KOs and NICs.* ***(C, J, Q)*** *Stroke volume expressed in nanoliters of the different genetic KOs and NICs.* ***(D, K, R)*** *Ejection fraction of the different genetic KOs and NICs.* ***(E, L, S)*** *Relative contractility measured in the fractional area change of the genetic KOs and NICs.* ***(F, M, T)*** *Relaxation time expressed in seconds of the different genetic KOs and NICs.* ***(G, N, U)*** *Contraction time expressed in seconds of the different genetic KOs and NICs.* ***(A-G)*** *Injection 1 (A: n = 22-36, B-G: 18-30).* ***(H-N)*** *Injection 2 (H: n =26-42, I-N: n = 18-32).* ***(O-U)*** *Injection 3 (O: n = 30-35, P-U: n =22-30). *p<0.05, **p<0.01, ***p<0.001. laptm4b, lysosomal-associated transmembrane protein 4 beta; pigv, phosphatidylinositol glycan anchor biosynthesis class V ; ankhd1, ankyrin repeat and KH domain containing 1.*

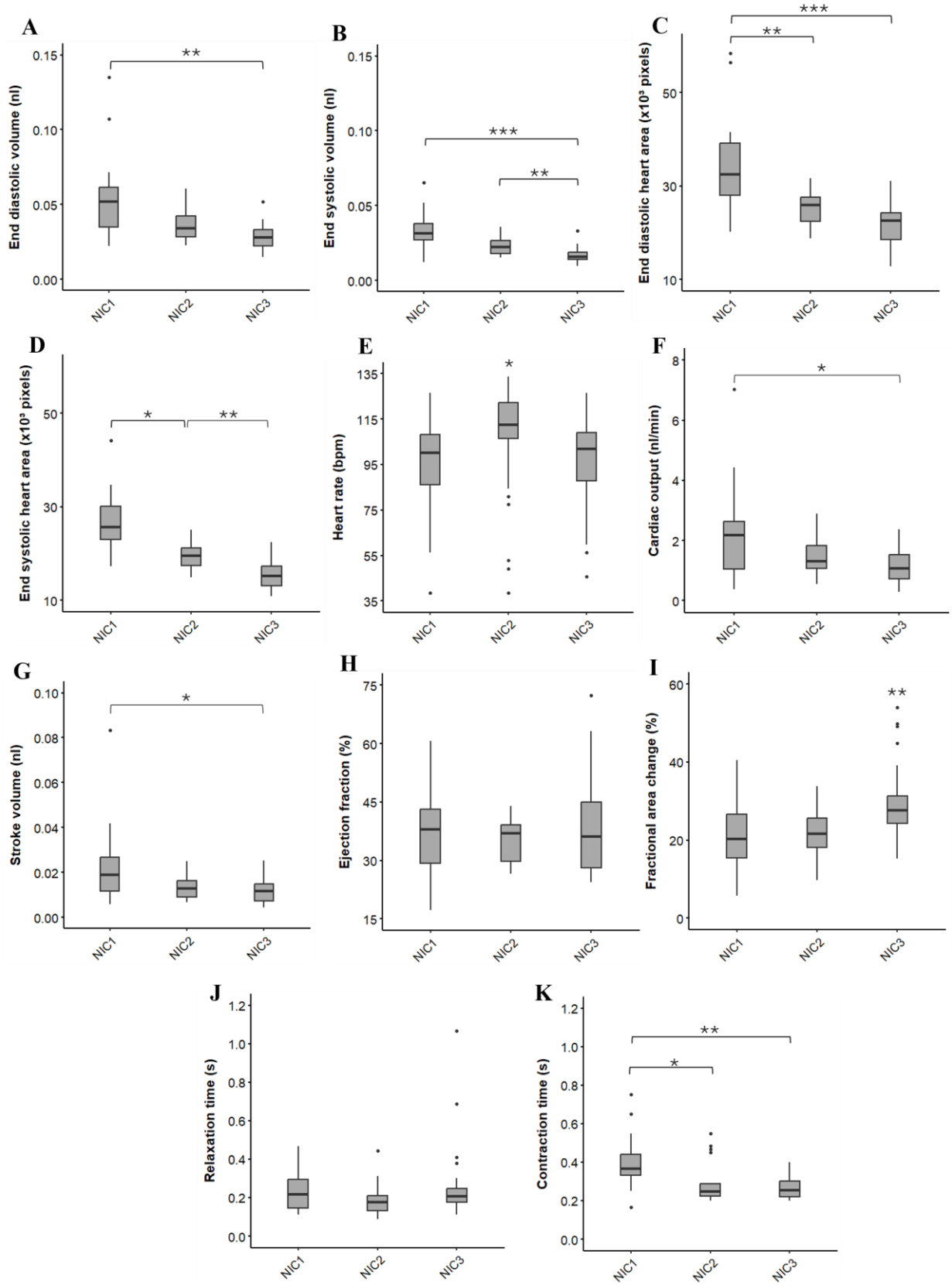
A
End diastolic volume (nl)
0.15
0.10
0.05
0.00
**
NIC1
NIC2
NIC3
B
End systolic volume (nl)
0.15
0.10
0.05
0.00
***
**
NIC1
NIC2
NIC3
C
End diastolic heart area (x10³ pixels)
50
30
10
***
**
NIC1
NIC2
NIC3
D
End systolic heart area (x10³ pixels)
50
30
10
*
**
NIC1
NIC2
NIC3
E
Heart rate (bpm)
135
115
95
75
55
35
*
NIC1
NIC2
NIC3
F
Cardiac output (nl/min)
8
6
4
2
0
*
NIC1
NIC2
NIC3
G
Stroke volume (nl)
0.10
0.08
0.06
0.04
0.02
0.00
*
NIC1
NIC2
NIC3
H
Ejection fraction (%)
75
60
45
30
15
NIC1
NIC2
NIC3
I
Fractional area change (%)
60
40
20
0
**
NIC1
NIC2
NIC3
J
Relaxation time (s)
1.2
1.0
0.8
0.6
0.4
0.2
0.0
NIC1
NIC2
NIC3
K
Contraction time (s)
1.2
1.0
0.8
0.6
0.4
0.2
0.0
**
*
NIC1
NIC2
NIC3

Figure S5 – Functional and ventricle size parameters of the different non-injected controls (NICs). *Wild type zebrafish eggs were injected with three gRNA targets to ensure disruption of either laptm4b, pigv, or ankhd1 in the F0 generation. At 3dpf embryos were anesthetized and videos were made of the ventricle to extract heart function and ventricle size parameters.* ***(A)*** *End diastolic volume expressed in nanoliter.* ***(B)*** *End systolic volume expressed in nanoliters.* ***(C)*** *End diastolic heart area expressed in x10³ pixels.* ***(D)*** *End systolic heart area expressed in x10³ pixels.* ***(E)*** *Heart rate expressed in beats per minute (bpm).* ***(F)*** *Cardiac output expressed in nanoliter per minute (nl/min).* ***(G)*** *Stroke volume expressed in nanoliters.* ***(H)*** *Ejection fraction expressed in percentage.* ***(I)*** *Relative contractility expressed as the fractional area change.* ***(J)*** *Relaxation time expressed in seconds.* ***(K)*** *Contraction time expressed in seconds. NIC1 (n = 18-22), NIC2 (n = 18-26), NIC3 (n = 28-35).*p<0.05, **p<0.01, ***p<0.001. NIC, non-injected control; laptm4b, lysosomal-associated transmembrane protein 4 beta; pigv, phosphatidylinositol glycan anchor biosynthesis class V ; ankhd1, ankyrin repeat and KH domain containing 1.*

Table S5 – Statistical summary.

Figure	Normal distributed	Equal variances	Statistical test	p-values
Fig. 4J – Phenotypes	/	/	Fisher's exact test with Pearson's residuals	A: p = 0.00001*** L: p = 0.00001*** P: p = 0.00001*** T: p = 0.00001***
Fig. 5A – EDV	No	No	Welch's t-test (n>30) + Bonferroni	A : p = 0.133 L : p = 1.000 P : p = 0.071
Fig. 5B – ESV	No	No	Welch's t-test (n>30) + Bonferroni	A: p = 0.099 L: p = 1.000 P: p = 0.006**
Fig. 5C – EDA	*laptm4b* : Yes NIC, *pigv*, *ankhd1* : No	No	Welch's t-test (n>30) + Bonferroni	A: p = 0.027* L: p = 1.000 P: p= 0.029*
Fig. 5D – ESA	*pigv* : Yes NIC, *laptm4b*, *ankhd1* : No	No	Welch's t-test (n>30) + Bonferroni	A : p = 0.034* L : p = 1.000 P: p = 0.009**
Fig. 6A – HR	No	No	Welch's t-test (n>30) + Bonferroni	A: p = 1.000 L : p = 0.000022*** P: p = 1.000
Fig. 6B – CO	No	Yes	Wilcoxon rank sum + Bonferroni	A: p = 0.483 L: p = 1.000 P: p = 1.000
Fig. 6C – SV	No	No	Welch's t-test (n>30) + Bonferroni	A: p = 0.271 L: p = 0.423 P: p = 1.000
Fig. 6D – EF	*pigv*, *laptm4b, ankhd1* : Yes NIC : No	Yes	Wilcoxon Rank sum test + Bonferroni	A: p = 0.816 L: p = 0.035* P: p = 0.099
Fig. 6E – RT	No	Yes	Wilcoxon Rank sum test + Bonferroni	A: p = 1.000 L: p = 0.348 P: p = 0.045*
Fig. 6F – CT	No	No	Welch's t-test (n>30) + Bonferroni	A: p = 0.384 L: p = 0.390 P: p = 1.000
Fig. 6G – FAC	*laptm4b, pigv, ankhd1* : Yes NIC : No	Yes	Wilcoxon Rank sum + Bonferroni	A: p = 1.000 L: p = 0.284 P: p = 0.309

Fig. S3A – EDV	*laptm4b* : Yes NIC, *ankhd1* : No	Yes	Wilcoxon Rank sum test + Bonferroni	A : p = 1.000 L : p = 1.000
Fig.S3B – ESV	NIC, *laptm4b* : Yes *ankhd1* : No	Yes	L : Unpaired t-test A : Wilcoxon Rank sum test + Bonferroni	A : p = 1.000 L : p = 0.59
Fig. S3C – EDA	*laptm4b* : Yes NIC, *ankhd1* : No	Yes	Wilcoxon Rank sum test + Bonferroni	A : p = 1.000 L : p = 1.000
Fig. S3D – ESA	NIC, *laptm4b* : Yes *ankhd1* : No	Yes	L : Unpaired t-test A : Wilcoxon Rank sum test + Bonferroni	A : p = 1.000 L : p = 0.23
Fig. S3E – EDV	Yes	Yes	Unpaired t-test + Bonferroni	A : p = 1.000 P : p = 1.000
Fig. S3F – ESV	NIC, *pigv*: Yes *ankhd1*: No	Yes	A : Wilcoxon Rank sum test P : Unpaired t-test + Bonferroni	A : p = 0.856 P : p = 0.041*
Fig. S3G – EDA	NIC, *pigv* : Yes *ankhd1* : No	Yes	A : Wilcoxon Rank sum test P : Unpaired t-test + Bonferroni	A : p = 1.000 P : p = 0.954
Fig. S3H – ESA	NIC, *pigv* : Yes *ankhd1* : No	Yes	A : Wilcoxon Rank sum test P : Unpaired t-test + Bonferroni	A : p = 0.424 P : p = 0.05 *
Fig. S3I – EDV	Yes	Yes	Unpaired t-test + Bonferroni	L : p = 1.000 P : p = 1.000
Fig. S3J – ESV	*pigv :* Yes NIC, *laptm4b* : No	Yes	A : Wilcoxon Rank sum test P: Unpaired t-test + Bonferroni	L : p = 1.000 P : p = 1.000
Fig. S3K - EDA	Yes	Yes	Unpaired t-test + Bonferroni	L : p = 1.000 P : p = 1.000
Fig. S3L - ESA	Yes	Yes	Unpaired t-test + Bonferroni	L : p = 1.000 P : p = 0.406
Fig. S4A - HR	NIC : Yes *laptm4b, ankhd1:* No	No	Wilcoxon Rank sum test + Bonferroni	A : p = 1.000 L : p = 0.157
Fig. S4B – CO	*laptm4b* : Yes NIC, *ankhd1* : No	Yes	Wilcoxon Rank sum test + Bonferroni	A : p = 1.000 L : p = 1.000
Fig. S4C – SV	No	Yes	Wilcoxon Rank sum test + Bonferroni	A : p = 1.000 L : p = 0.442
Fig. S4D – EF	Yes	Yes	Unpaired t-test + Bonferroni	A : p = 1.000 L : p = 0.147
Fig. S4E – FAC	Yes	No	Welch's test + Bonferroni	A : p = 0.274 L : p = 0.011*
Fig. S4F – RT	NIC : Yes *ankhd1, laptm4b* : No	Yes	Wilcoxon Rank sum test + Bonferroni	A : p = 1.000 L : p = 0.69
Fig. S4G - CT	NIC, *ankhd1* : Yes *laptm4b* : No	No	A : Welch's test L : Wilcoxon Rank sum test + Bonferroni	A : p = 0.012* L : p = 0.179
Fig. S4H – HR	No	Yes	Wilcoxon Rank sum test + Bonferroni	A : p = 0.362 P : p = 0.902
Fig. S4I – CO	NIC: Yes *pigv, ankhd1* : No	Yes	Wilcoxon Rank sum test + Bonferroni	A : p = 1.000 P : p = 1.000
Fig. S4J – SV	NIC, *ankhd1* : Yes *pigv* : No	Yes	A : Unpaired t-test P : Wilcoxon Rank sum test + Bonferroni	A : p = 0.428 P : p = 1.000

Fig. S4K – EF	Yes	No	Welch's test + Bonferroni	A : p = 0.110 P : p = 0.002 **
Fig. S4L – FAC	Yes	No	Welch's test + Bonferroni	A : p = 0.18 P : p = 0.01 **
Fig. S4M – RT	No	Yes	Wilcoxon Rank sum test + Bonferroni	A : p = 1.000 P : p = 1.000
Fig. S4N – CT	No	Yes	Wilcoxon Rank sum test + Bonferroni	A : p = 1.000 P : p = 0.86
Fig. S4O – HR	No	No	Welch's test (n>30) + Bonferroni	L : p = 0.004 ** P : p = 1.000
Fig. S4P – CO	Yes	Yes	Unpaired t-test + Bonferroni	L : p = 0.698 P : p = 0.348
Fig. S4Q – SV	Yes	Yes	Unpaired t-test + Bonferroni	L : p = 1.000 P : p = 1.000
Fig. S4R – EF	*laptm4b, pigv* : Yes NIC : No	Yes	Wilcoxon Rank sum test + Bonferroni	L : p = 0.658 P : p = 1.000
Fig. S4S – FAC	*laptm4b, pigv* : Yes NIC : No	Yes	Wilcoxon Rank sum test + Bonferroni	L : p = 0.348 P : p = 0.190
Fig. S4T – RT	*pigv* : Yes *laptm4b*, NIC : No	Yes	Wilcoxon Rank sum test + Bonferroni	L : p = 1.000 P : p = 0.085
Fig. S4U – CT	No	No	Wilcoxon Rank sum test + Bonferroni	L : p = 0.000906*** P : p = 0.000212***
Fig. S5A – EDV	NIC1 : No NIC2&3 : Yes	No	Kruskal-Wallis test with Dunn's post hoc comparisons	NIC1-2 : p = 0.090876 NIC1-3 : p = 0.000009*** NIC2-3 : p = 0.06755
Fig. S5B – ESV	NIC1&2 : Yes NIC3 : No	No	Kruskal-Wallis test with Dunn's post hoc comparisons	NIC1-2 : p = 0.11102 NIC1-3 : p = 0.0000005*** NIC2-3 : p = 0.00963**
Fig. S5C – EDA	NIC1 : No NIC2&3 : Yes	No	Kruskal-Wallis test with Dunn's post hoc comparisons	NIC1-2 : p = 0.007227** NIC1-3 : p = 1.888e-07*** NIC2-3 : p = 0.117596
Fig. S5D – ESA	Yes	No	Kruskal-Wallis test with Dunn's post hoc comparisons	NIC1-2 : p = 0.01218* NIC1-3 : p = 5.2298e-10 NIC2-3 : p = 0.003954**
Fig. S5E – HR	NIC1 : Yes NIC2&3 : No	Yes	Kruskal-Wallis test with Dunn's post hoc comparisons	NIC1-2 : p = 0.03892* NIC1-3 : p = 1.000 NIC2-3 : p = 0.02999*
Fig. S5F – CO	NIC1 : No NIC2&3 : Yes	Yes	Kruskal-Wallis test with Dunn's post hoc comparisons	NIC1-2 : p = 0.51246 NIC1-3 : p = 0.01895* NIC2-3 : p = 0.66766
Fig. S5G – SV	NIC1 : No NIC2&3 : Yes	No	Kruskal-Wallis test	NIC1-2 : p = 0.22899 NIC1-3 : p = 0.01052* NIC2-3 : p = 1.000
Fig. S5H – EF	NIC1&2 : Yes NIC3 : No	Yes	Kruskal-Wallis test	p = 0.9271
Fig. S5I - FAC	NIC1&2 : Yes NIC3 : No	No	Kruskal-Wallis test with Dunn's post hoc comparisons	NIC1-2 : p = 1.000 NIC1-3 : p = 0.0022** NIC2-3 : p = 0.0049**
Fig. S5J – RT	NIC1 : Yes NIC2&3 : No	Yes	Kruskal-Wallis test	p = 0.3011

Fig. S5K – CT	NIC1 : Yes NIC2&3 : No	No	Kruskal-Wallis test with Dunn's post hoc comparisons	NIC1-2 : p = 0.01707* NIC1-3 : p = 0.002418** NIC2-3 : p = 1.000

Table S6 – Pearson's residuals of Phenotypic proportions.

	Normal	*In chorion*	*Mild to moderate edema*	*Severe edema*	*Severe malformation*	*tmpk phenotype*
laptm4b	-11.28	1.78	10.68	1.25	2.55	/
pigv	-12.6	1.11	11.75	3.02	3.44	/
ankhd1	-10.07	-0.63	10.78	2.87	2.65	/
tmpk	-6.12	0.03	-3.22	-0.66	-1.46	24.43